Supporting Information

Design Syntheses of Metal-organic Layer with Rich N-sites for CO_2 Chemical Fixation

Zhi-Wen Wang[a,b], Zi-Yi Zhu[b], Shangda Li[b,*], Fei Wang[b,*]

1. Experimental

1.1 Chemicals and Methods

1.1.1 Chemicals

All chemicals and solvents were used without further purification. L-lactic acid (99%+, damas-beta), D-lactic acid (99%, damas-beta), O-Phenylene diamine (OPD, 99%, damas-beta), Sodium Hydroxide (NaOH, AR, XiLong Scientific), Terephthalic Acid (BDC, 99%, damas-beta), Zinc nitrate hexahydrate ($Zn(NO_3)_2 \cdot 6H_2O$, AR, HUSHI), N, N-Dimethylformamide (DMF, AR, HUSHI), Methanol (MeOH, AR, HUSHI), Water (H_2O, AR, Macklin), Hydrochloric Acid (HCl, AR, HUSHI), Sodium hydroxide aqueous solution (1M NaOH, ANPEL).

1.1.2 Methods

IR spectra:

IR spectra (KBr pellets) were recorded on an ABB Bomem MB102 spectrometer over a range of 400-4000 cm^{-1}.

Powder X-ray diffraction:

Powder X-ray diffraction (PXRD) data were collected on a Rigaku Mini Flex II diffractometer using CuKα radiation (λ = 1.54056 Å) under ambient conditions.

Thermogravimetric analyses:

The thermogravimetric analyses (TGA) were performed on a Mettler Toledo TGA/SDTA 851e analyzer in a nitrogen atmosphere with a heating rate of 10 °C/min.

Solid circular dichroism spectra:

The spectra (KBr pellets) were recorded on a MOS-450 spectropolarimeter. The mixture of sample and 50 mg dry KCl powder was well-grounded and then pressed into a disk for the CD measurement.

Fluorescent (FL):

Fluorescence spectra were investigated by a fluorescent spectrophotometer (Edinburgh, FLS980).

Proton Nuclear Magnetic Resonance Spectroscopy (^{1}H NMR):

^{1}H NMR experiments were carried out on a Bruker spectrometer operating at resonance frequencies of 600 MHz.

1.2 Synthesis of Ligands

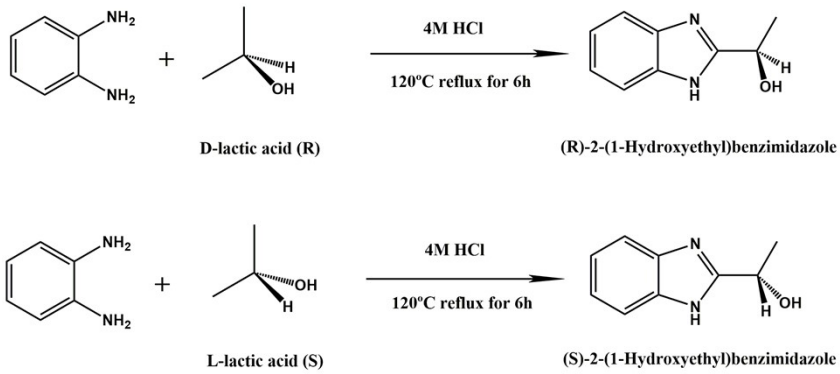

Scheme S1. The synthesis method of the OH-bim ligands.

Synthesis of (S)-2-(1-Hydroxyethyl)benzimidazole (S-OH-bim)：

This compound was prepared based on a known method with some modification. The mixture of o-phenylenediamine (64.9 g, 0.6 mol) and L-lactic acid (58.26 mL, 0.78 mol) in 600 mL 4 M HCl were stirred and heated to reflux for 6 hours under 120 ℃. Then slowly cooled and the resultant mixture was basified with aqueous sodium hydroxide solution. The solution was then neutralized with NaOH to afford the product as a brownish solid in 60% yield.

Synthesis of (R)- 2-(1-Hydroxyethyl)benzimidazole (R-OH-bim):

The R-ligand was obtained by the similar method as described for using (R)-lactic acid instead of (S)-lactic acid (Yield: 55%).

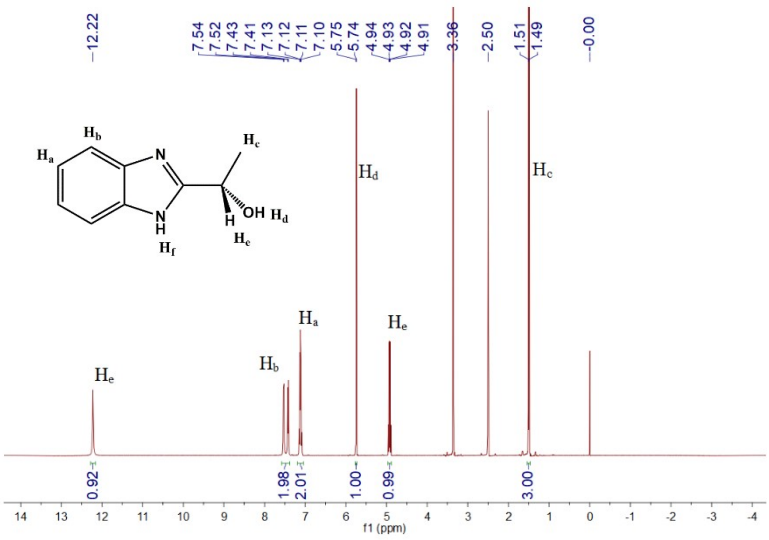

Figure S1. 600 MHz ^{1}H NMR spectrum of S-OH-bim in DMSO-D_6.

1.3 Synthesis of MOFs

Synthesis of S-1-Zn:

S-OH-bim (0.081 g, 0.5 mmol), H_2BDC (0.083 g, 0.5 mmol), $Zn(NO_3)_2 \cdot 6H_2O$ (0.150 g, 0.5 mmol), N, N-Dimethylformamide (2 mL), methanol (2 mL), deionized water (2 mL) was sealed in a 20 mL vial and heated to 100 ℃ for one day. After cooling to room temperature, the colorless crystals were obtained in the pure phase.

Synthesis of R-1-Zn:

It was obtained by the similar method as described for S-1-Zn except for using R-OH-bim instead of S-OH-bim.

Synthesis of S-1-Cd:

S-OH-bim (0.032g, 0.2mmol), H_2BDC (0.032 g, 0.2 mmol), $CdCl_2 \cdot 5/2H_2O$ (0.068 g, 0.3 mmol), deionized water (2 mL), methanol (3 mL) and NaOH aqueous solution (1M, 300 μL) was sealed in a 20 mL vial and heated to 80 ℃ for 3 days. After cooling to room temperature, the colorless crystals were obtained in the pure phase.

Synthesis of R-1-Cd:

It was obtained by the similar method as described for S-1-Cd except for using R-OH-bim instead of S-OH-bim.

Table S1. Crystal Data and Structure Refinement for S-1-Zn, R-1-Zn, S-1-Cd and R-1-Cd.

	S-1-Zn	**R-1-Zn**	**S-1-Cd**	**R-1-Cd**
Formula	$C_{44}H_{40}N_4O_{16}Zn_3$	$C_{44}H_{40}N_4O_{16}Zn_3$	$C_{44}H_{40}N_4O_{16}Cd_3$	$C_{44}H_{40}N_4O_{16}Cd_3$
Mr	1076.97	1076.97	1218.04	1218.04
Crystal system	orthorhombic	orthorhombic	orthorhombic	orthorhombic
Space group	$P2_12_12_1$	$P2_12_12_1$	$P2_12_12_1$	$P2_12_12_1$
a (Å)	11.17930(10)	11.18090(10)	11.52880(10)	11.52890(10)
b (Å)	15.0014(2)	15.00360(10)	11.52880(10)	15.10390(10)
c (Å)	25.5008(2)	25.50610(10)	26.5164(2)	26.52250(10)
β (deg)	90	90	90	90
V ($Å^3$)	4276.62(8)	4278.74(5)	4613.32(6)	4618.40(5)
Z	4	4	4	4
Dc ($g \cdot m^{-3}$)	1.666	1.665	1.748	1.742
μ (mm^{-1})	1.636	1.742	7.761	7.741
F (000)	2184	2184	2392	2388
Flack	0.017(13)	-0.005(7)	0.008(8)	-0.013(3)
R_{int}	0.0333	0.0198	0.0365	0.0376
GOF (F^2)	1.049	1.082	1.064	1.014
R_1 ($I > 2\sigma(I)$)	0.0326	0.0278	0.0449	0.0205
wR_2 ($I > 2\sigma(I)$)	0.0801	0.0706	0.122	0.0508
R_1 (all data)	0.035	0.0293	0.0461	0.0224
wR_2 (all data)	0.0819	0.071	0.123	0.0516
CCDC No.	2123927	2123925	2123926	2123924

Table S2. Hydrogen Bonds for S-1-Zn.

D	H	A	d(D-H)/Å	d(H-A)/Å	d(D-A)/Å	D-H-A/°
O00H	H00H	O01O	0.84	1.81	2.621(6)	162.7
O00I	H00I	O00M	0.84	1.87	2.703(5)	172.1

N00K	H00K	O00B[1]	0.88	1.93	2.789(4)	166.4
N00L	H00L	O00E[2]	0.88	1.86	2.742(4)	176.2
O00M	H00M	O007[3]	0.84	2.00	2.836(5)	171.3

Symmetric operation code:[1]1/2-X,1-Y,1/2+Z; [2]3/2-X,1-Y,-1/2+Z; [3]-1+X,+Y,+Z

Table S3. Hydrogen Bonds for R-1-Zn.

D	H	A	d(D-H)/Å	d(H-A)/Å	d(D-A)/Å	D-H-A/°
O50	H50	O66	0.84	1.82	2.622(5)	159.0
O62	H62	O64	0.84	1.87	2.705(4)	173.6
N60	H60	O23[1]	0.88	1.93	2.793(4)	166.5
N41	H41	O11[2]	0.88	1.86	2.740(4)	175.9
O64	H64	O14[3]	0.84	2.06	2.834(4)	153.8

Symmetric operation code: [1]1/2-X,1-Y,-1/2+Z; [2]3/2-X,1-Y,1/2+Z; [3]-1+X,+Y,+Z

Table S4. Hydrogen Bonds for S-1-Cd.

D	H	A	d(D-H)/Å	d(H-A)/Å	d(D-A)/Å	D-H-A/°
N00E	H00E	O00J[1]	0.86	2.01	2.856(8)	169.8
O00F	H00F	O01B	0.858(13)	1.755(17)	2.591(8)	164(3)
O00K	H00K	O01F[2]	0.864(13)	1.73(2)	2.554(9)	160(4)
N017	H017	O005[3]	0.86	1.93	2.788(8)	174.5
O01B	H01T	O007[4]	0.82	1.98	2.760(8)	158.7
O01F	H01X	O00A	0.82	1.92	2.741(10)	173.3

Symmetric operation code: [1]1-X,-1/2+Y,3/2-Z;[2]1/2+X,1/2-Y,1-Z; [3]-X,1/2+Y,1/2-Z; [4]1/2+X,3/2-Y,1-Z

Table S5. Hydrogen Bonds for R-1-Cd.

D	H	A	d(D-H)/Å	d(H-A)/Å	d(D-A)/Å	D-H-A/°
N00A	H00A	O00I[1]	0.86	2.00	2.857(4)	171.1
O00E	H00E	O00Z	0.857(12)	1.754(14)	2.593(4)	166(3)
O00G	H00G	O01M	0.880(13)	1.695(14)	2.563(5)	168(3)
O00Z	H00Z	O006[2]	0.82	1.96	2.757(4)	164.0
N016	H016	O005[3]	0.86	1.95	2.802(4)	174.4
O01M	H01W	O008[4]	0.82	1.94	2.742(5)	167.7

Symmetric operation code: [1]-X,1/2+Y,1/2-Z; [2]1/2+X,1/2-Y,1-Z; [3]2-X,-1/2+Y,3/2-Z; [4]-1/2+X,3/2-Y,1-Z.

1.4 Characterizations

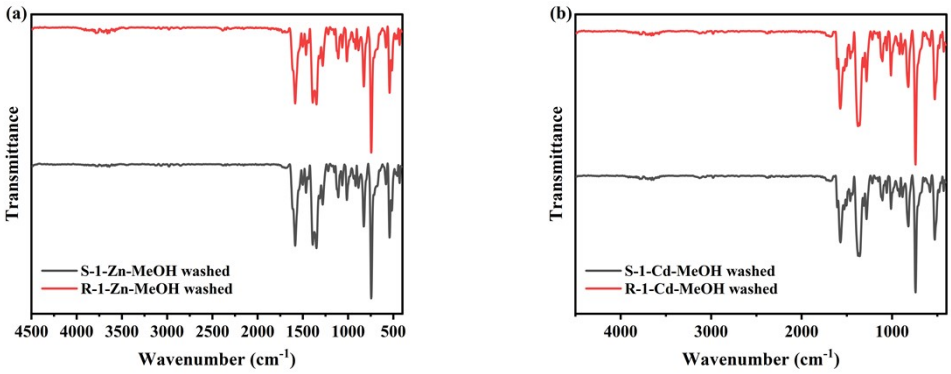

Figure S2. The IR spectra of (a) S/R-1-Zn, (b) S/R-1-Cd.

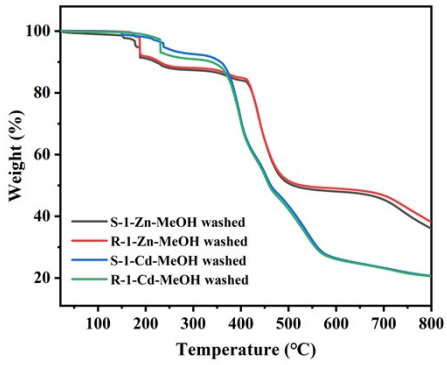

Figure S3. The TG plots of S/R-1-Zn and S/R-1-Cd.

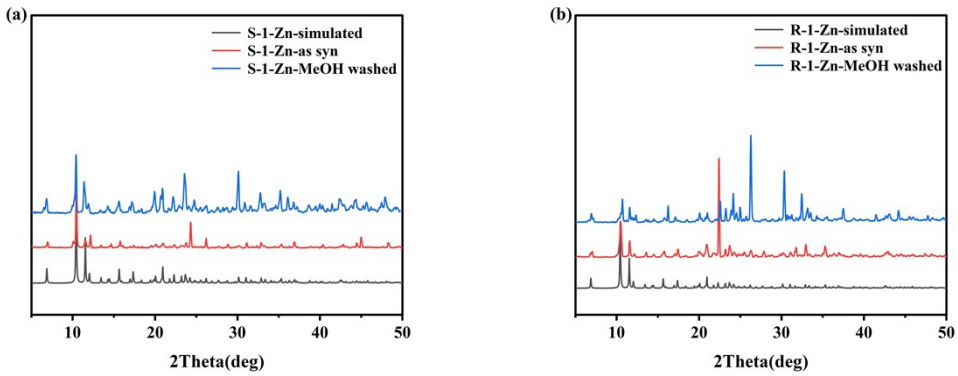

Figure S4. The powder XRD patterns of S/R-1-Zn under different conditions.

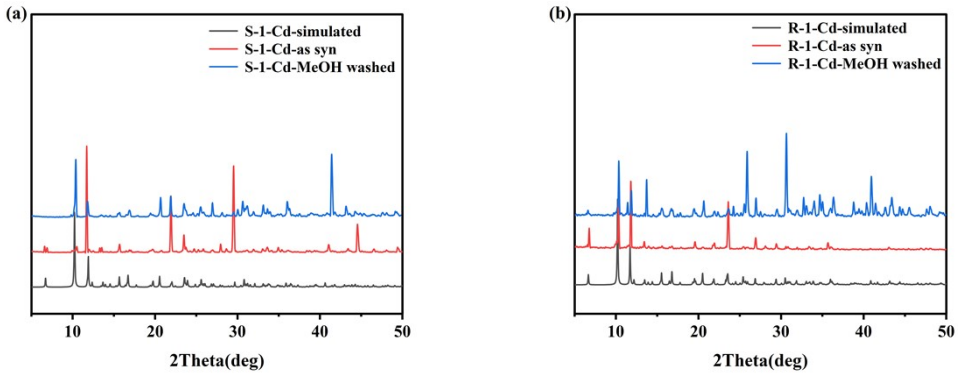

Figure S5. The powder XRD patterns of S/R-1-Cd under different conditions.

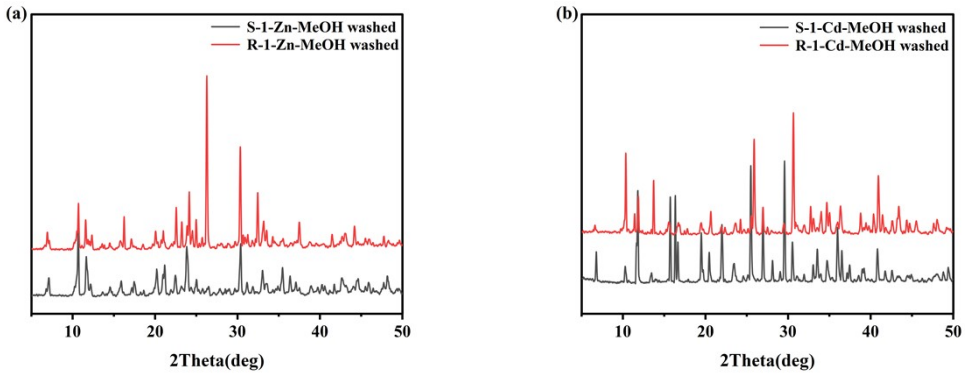

Figure S6. The powder XRD patterns of (a) S/R-1-Zn, (b) S/R-1-Cd.

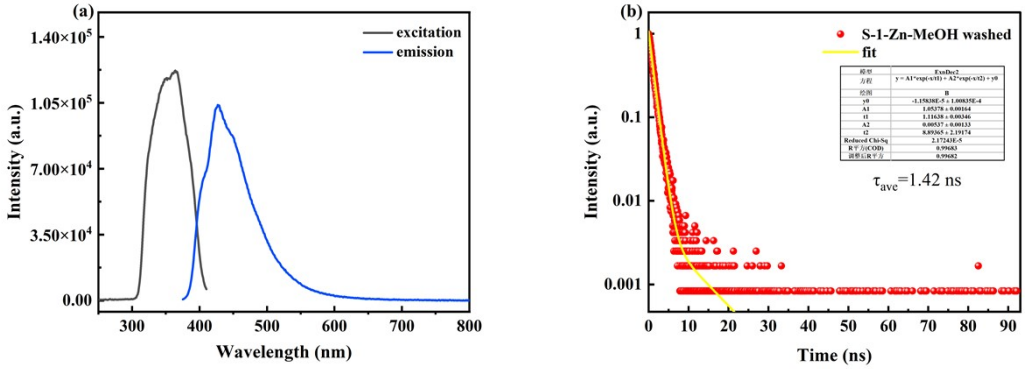

Figure S7. The Fl and Fl lifetime spectra of S-1-Zn.

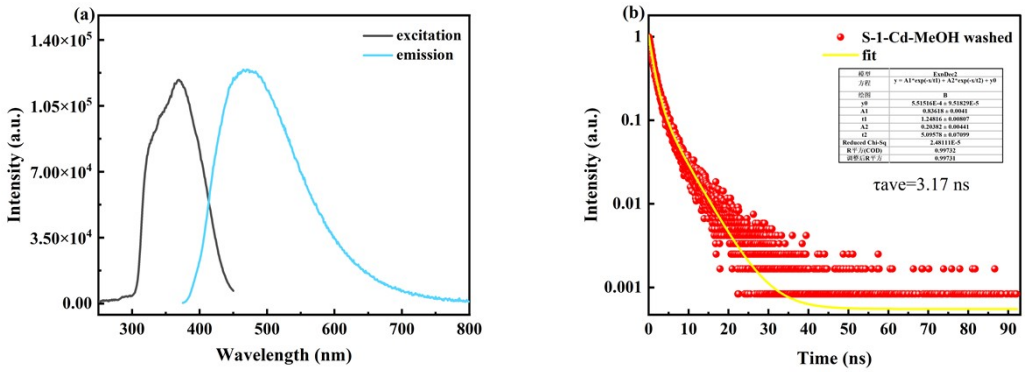

Figure S8. The Fl and Fl lifetime spectra of S-1-Cd.

1.5 Catalysis

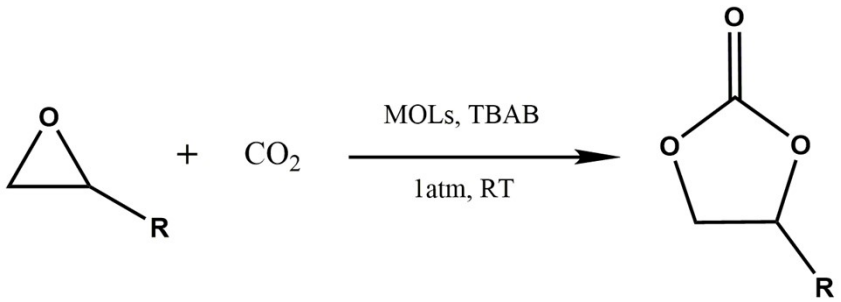

Scheme S2. 2D crystals-catalyzed cycloaddition of CO_2 and epoxides to form cyclic carbonates 1with TBAB as co-catalyst.

Exfoliation of 2D crystals: 760 mg of crystals were ground and taken in 30ml methanol, sonicated in a cell disrupter for 5 hours, the powder was obtained by filtration, rinsed with methanol, dried in the air for catalyst experimentation.

In each reaction, 20 mmol epoxide substrate, 80 mg catalyst (S-1-Zn/Cd or S-1-Zn/Cd-after spall), and 0.48 g tetra-n-tert-butylammonium bromide (TBAB) were mixed in a Schlenk tube. The Schlenk tube was solvent-free and purged with 1 atm CO_2 at room temperature for 8 h. The reaction mixture was then filtered, and the filtrate was characterized by ^{1}H NMR (600 MHz, $CDCl_3$) to study its conversion ratio. Between each run, the catalyst was recovered by filtration, rinsed with methanol, dried in the air, and reused on subsequent reactions without further treatment.

^{1}H NMR results

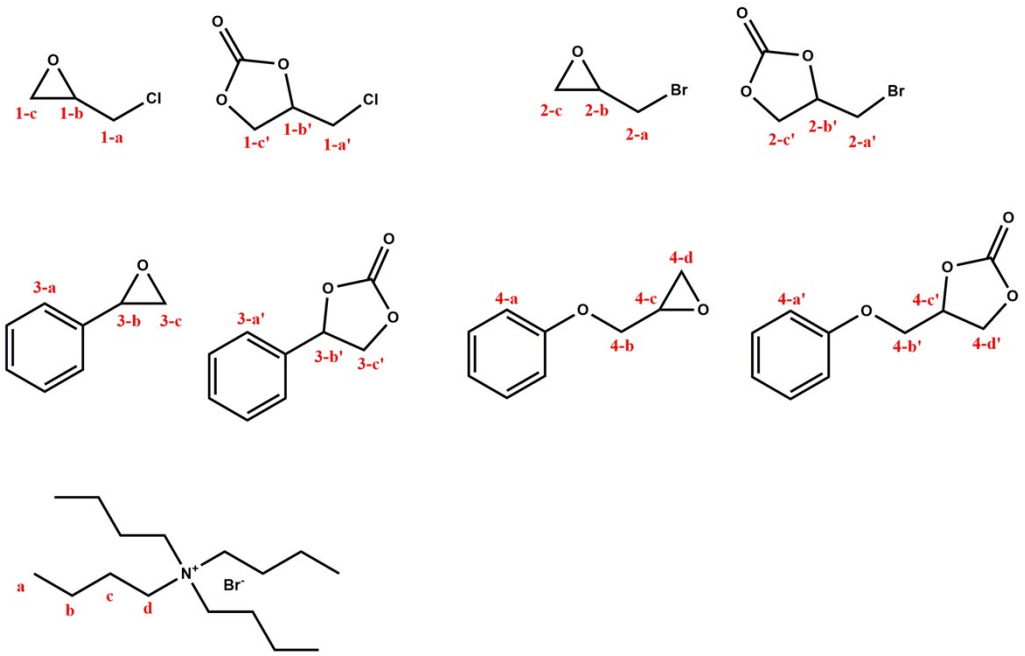

Figure S9. Hydrogen atom position in NMR analysis.

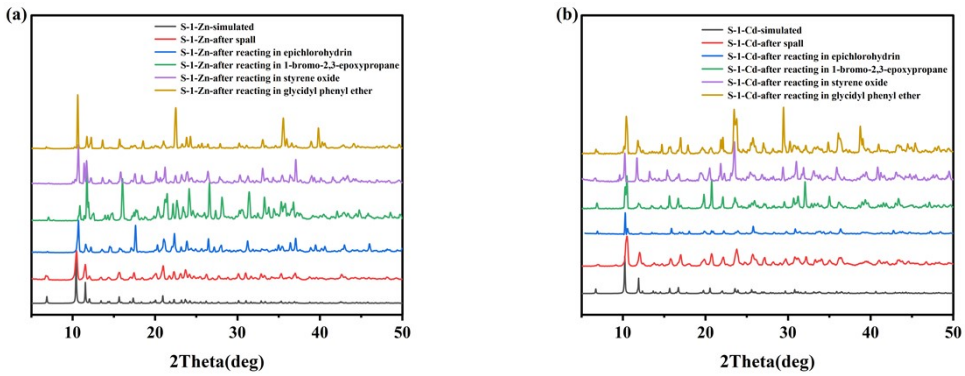

Figure S10. The powder XRD patterns of catalysis (a) S-1-Zn, (b) S-1-Cd.

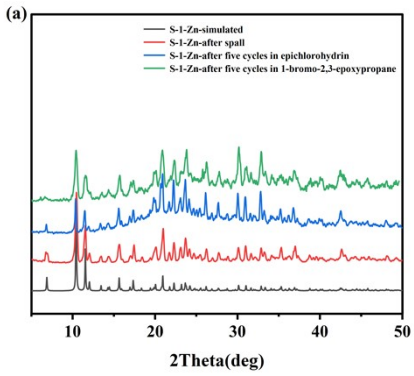

Figure S11. The powder XRD patterns of catalysis S-1-Zn as a catalyst after five cycles.

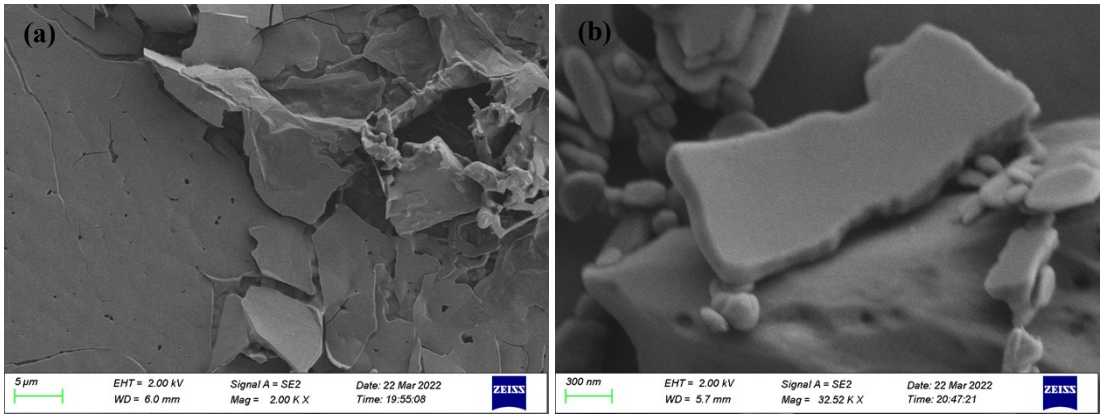

Figure S12. SEM image of (a) S-1-Zn-after spall, (b) S-1-Cd-after spall.

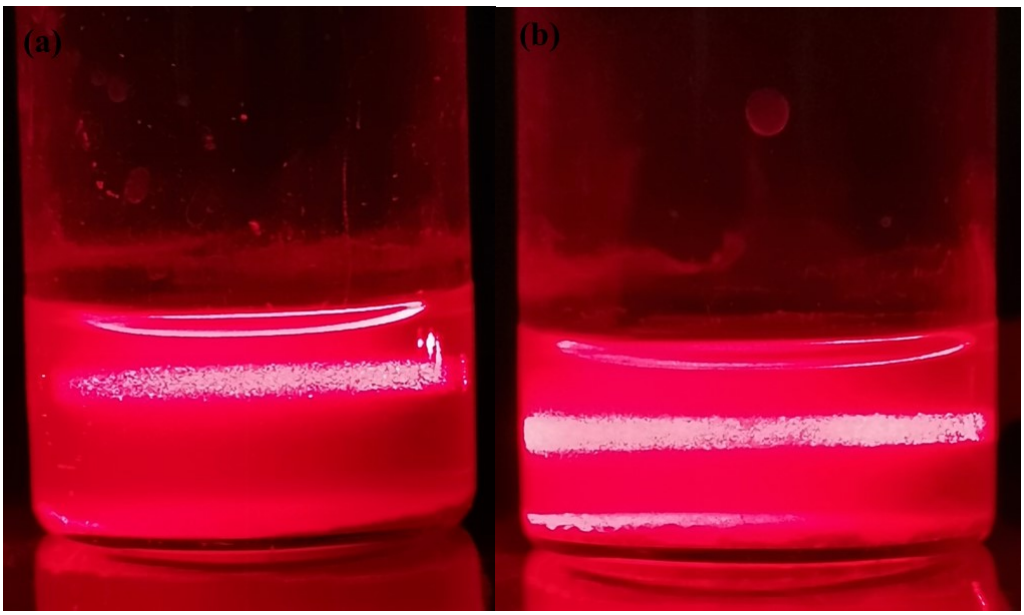

Figure S13. Tyndall phenomenon of (a) S-1-Zn-after spall, (b) S-1-Cd-after spall.

Table S6. A comparison table of the catalytic performance of the MOLs with other MOFs (1-Bromo-2,3-epoxypropane as substrate).

Entry	Compounds	Temp.	Time (h)	Co-catalyst	Con. [%]	Ref.
1	Ba-MOF	RT	48	TBAB	94.5	[1]
2	Nd-TTCA	333K	48	TBAB	95	[2]
3	GO	373K	12	/	＞99.9	[3]
4	$[Zn_2(TCA)(BIB)_{2.5}]\cdot(NO_3)$	353K	4	TBAB	＞99	[4]
5	$[In_2(L)(OH)_2]\cdot 2DMF\cdot 2H_2O$	343K	12	TBAB	99	[5]
6	$[Cu_2(L)(4,4'bipy)(OH)]\cdot H_2O$	353K	6	TBAB	91.7	[6]
7	$Ti_8O_8(OH)_4(bdc\text{-}NH_2)_6$	373K	2	TBAB	86.4	[7]
8	Al(III)@cage	RT	48	TBAB	87	[8]
9	$C_{48}H_{90}Al_2Li_4N_8$	327k	24	TBAB	85	[9]
10	$Cu_4[(C_{57}H_{32}N_{12})(COO)_8$	RT	48	TBAB	88	[10]
11	HKUST-1	RT	48	TBAB	57	[10]
12	S-1-Zn-after spall	RT	24	TBAB	84	This work

Imidazole is amphoteric, the uncoordinated N-H group on the OH-bim acts as a Brønsted acid to coordinate with the epoxide substrate, making it subject to nucleophilic attack by a cocatalyst (e.g., usually a tetraalkylammonium halide). The resulting halo alkoxide intermediates react with carbon dioxide to form cyclic carbonates, which then regenerate catalysts and cocatalysts [10,11]. The uncoordinated N-H groups can also act as Lewis basic sites, which can improve the affinity for carbon dioxide [12].

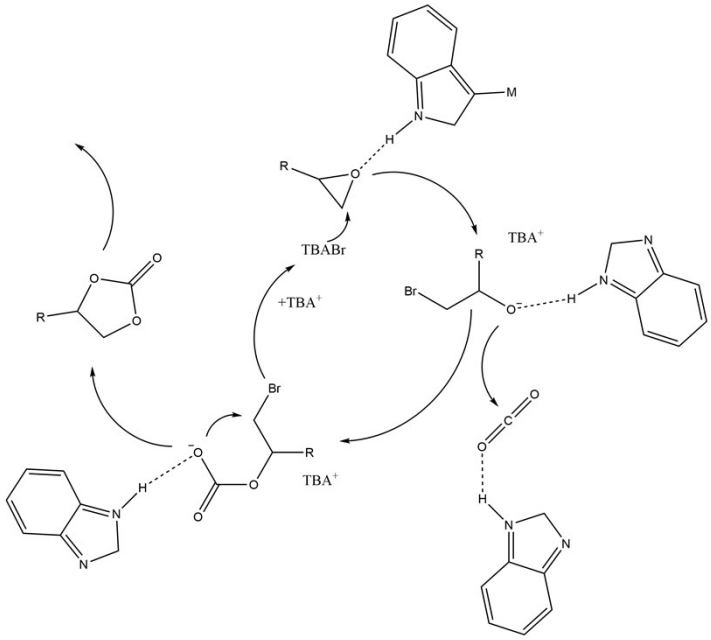

Figure S14. The proposed mechanism for the cycloaddition reaction catalyzed by MOLs.

At room temperature, 30mg S-1-Zn was soaked in 5 ml of solution for seven days, such as: methanol, ethanol, acetonitrile, acetone, DMF, DCM, NaOH aqueous solution (pH=13), HCl aqueous solution (pH=1), The stability was proved by P-XRD (Figure S15).

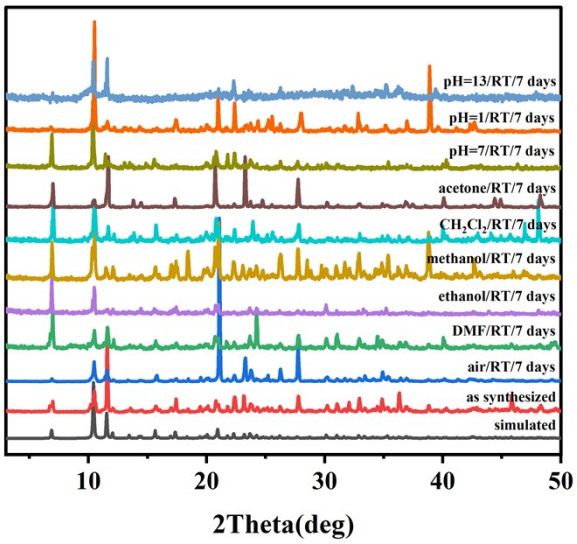

Figure S15. Powder XRD patterns of S-1-Zn under different conditions.

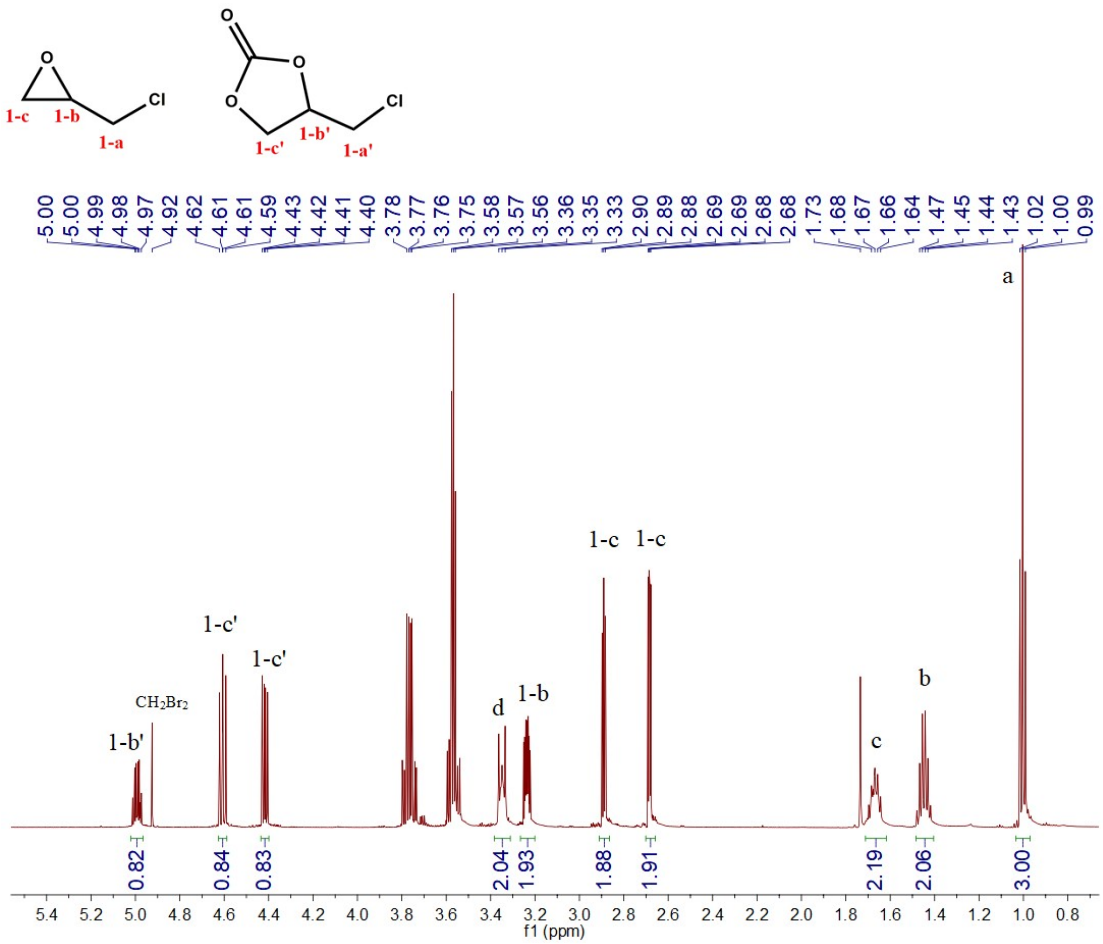

Figure S16. The first run of S-1-Zn-crystal as a catalyst in epichlorohydrin.

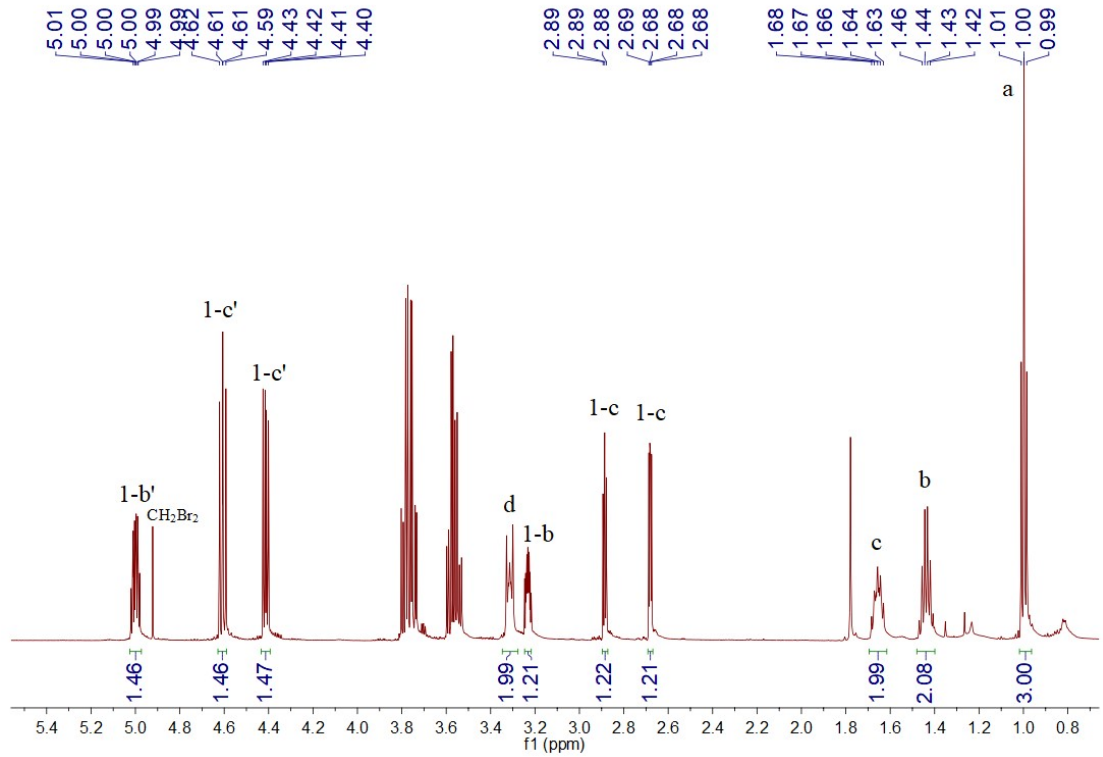

Figure S17. The first run of S-1-Zn-after spall as a catalyst in epichlorohydrin.

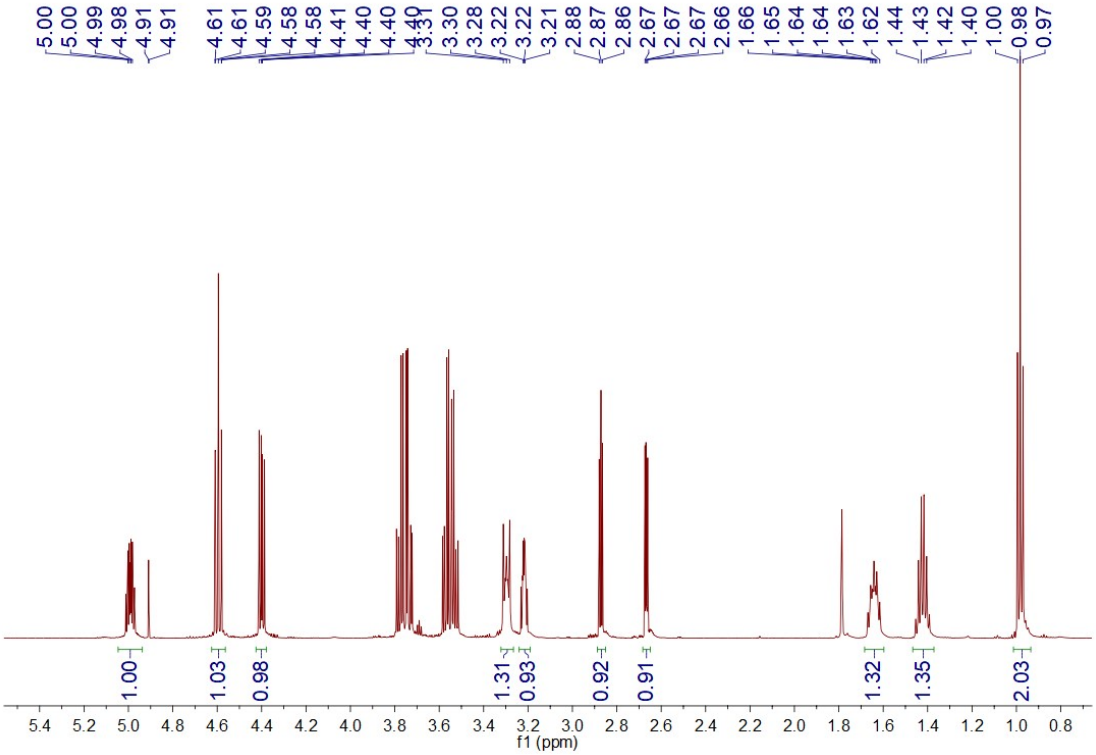

Figure S18. The second run of S-1-Zn-after spall as a catalyst in epichlorohydrin.

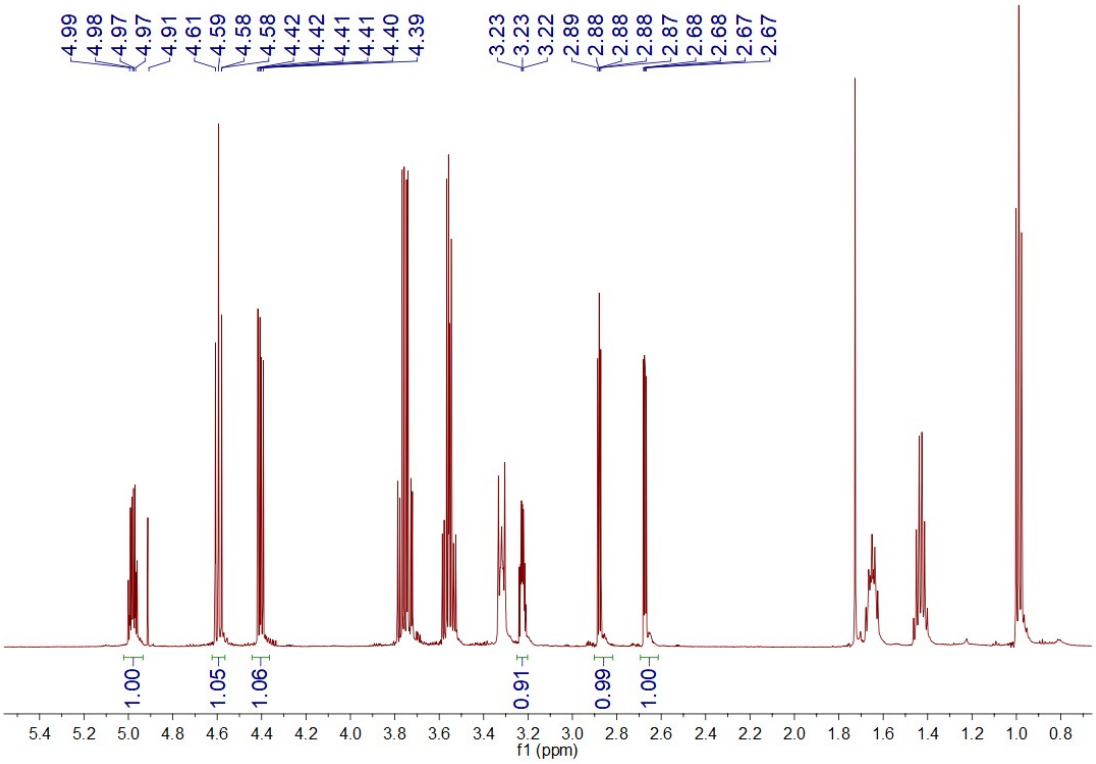

Figure S19. The third run of S-1-Zn-after spall as a catalyst in epichlorohydrin.

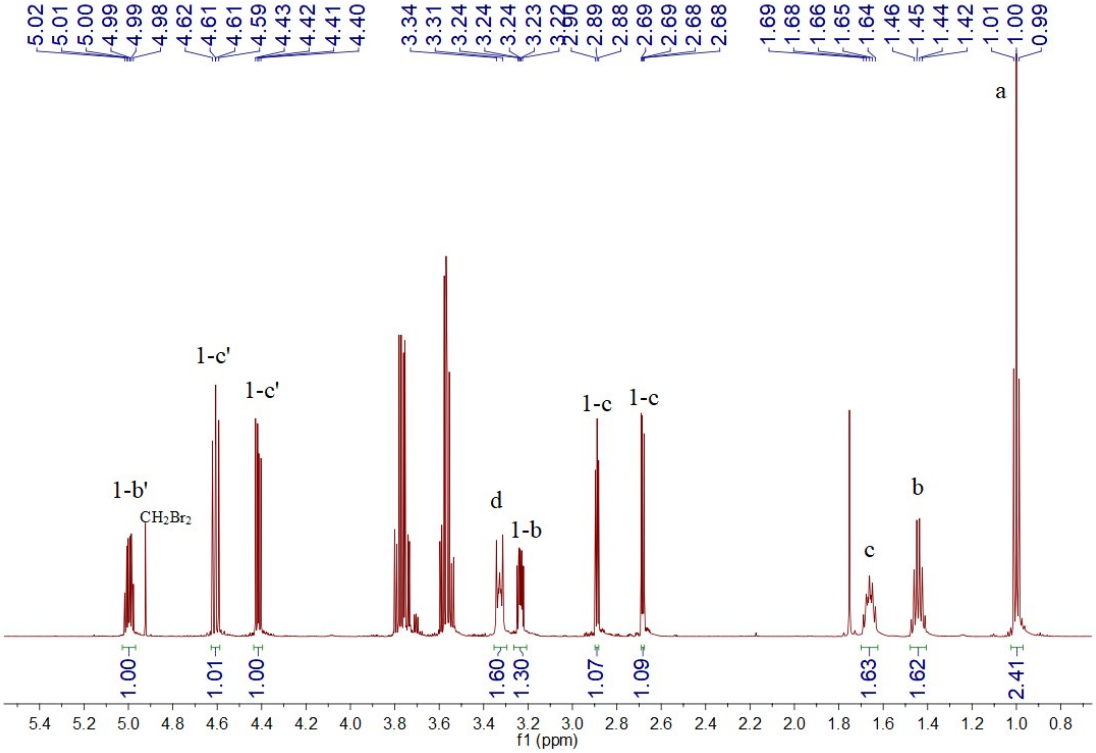

Figure S20. The fourth run of S-1-Zn-after spall as a catalyst in epichlorohydrin.

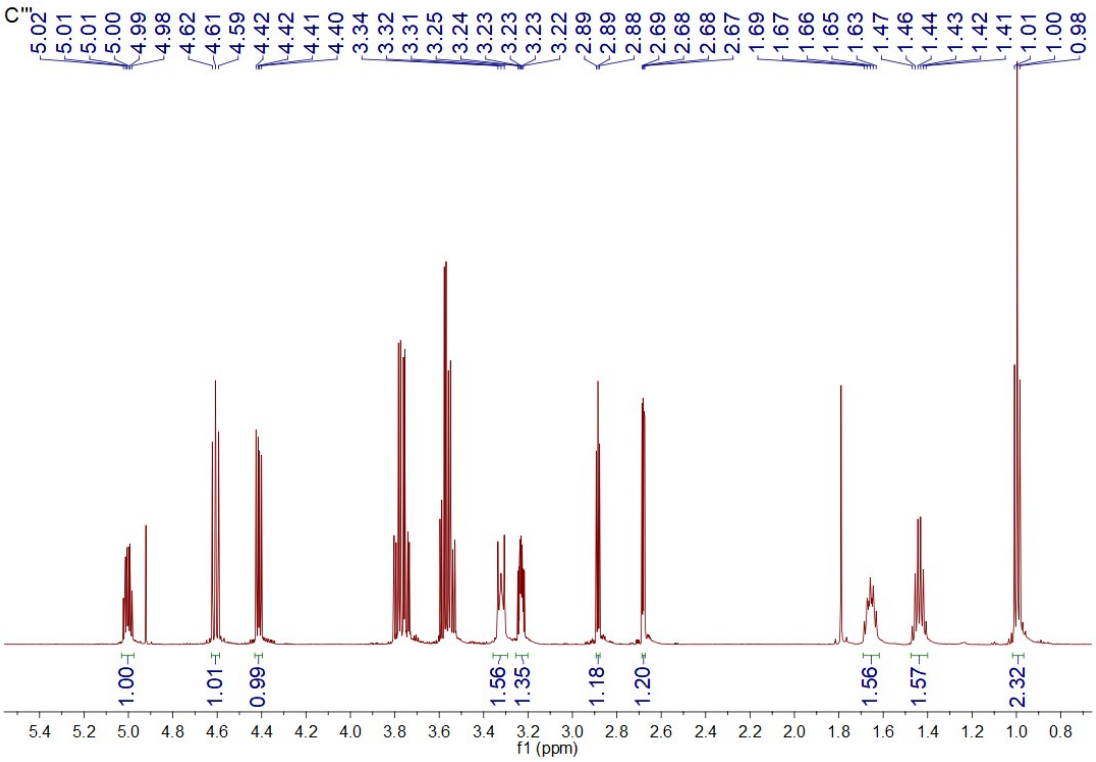

Figure S21. The fifth run of S-1-Zn-after spall as a catalyst in epichlorohydrin.

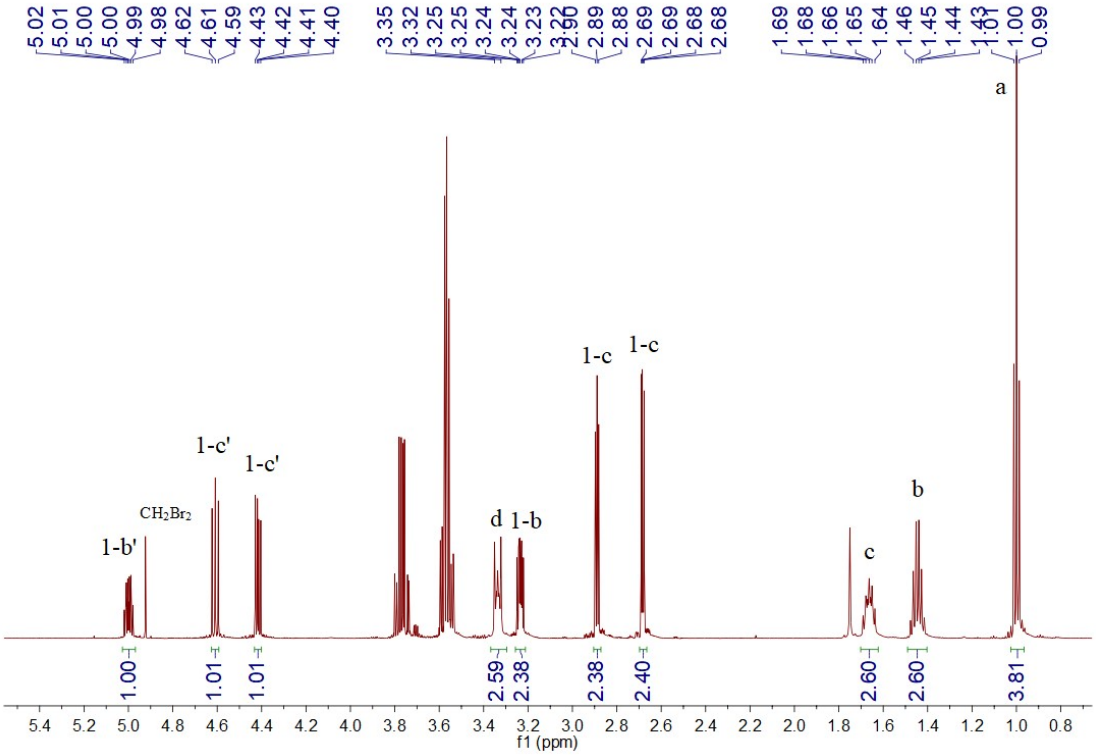

Figure S22. The first run of S-1-Cd-crystal as a catalyst in epichlorohydrin.

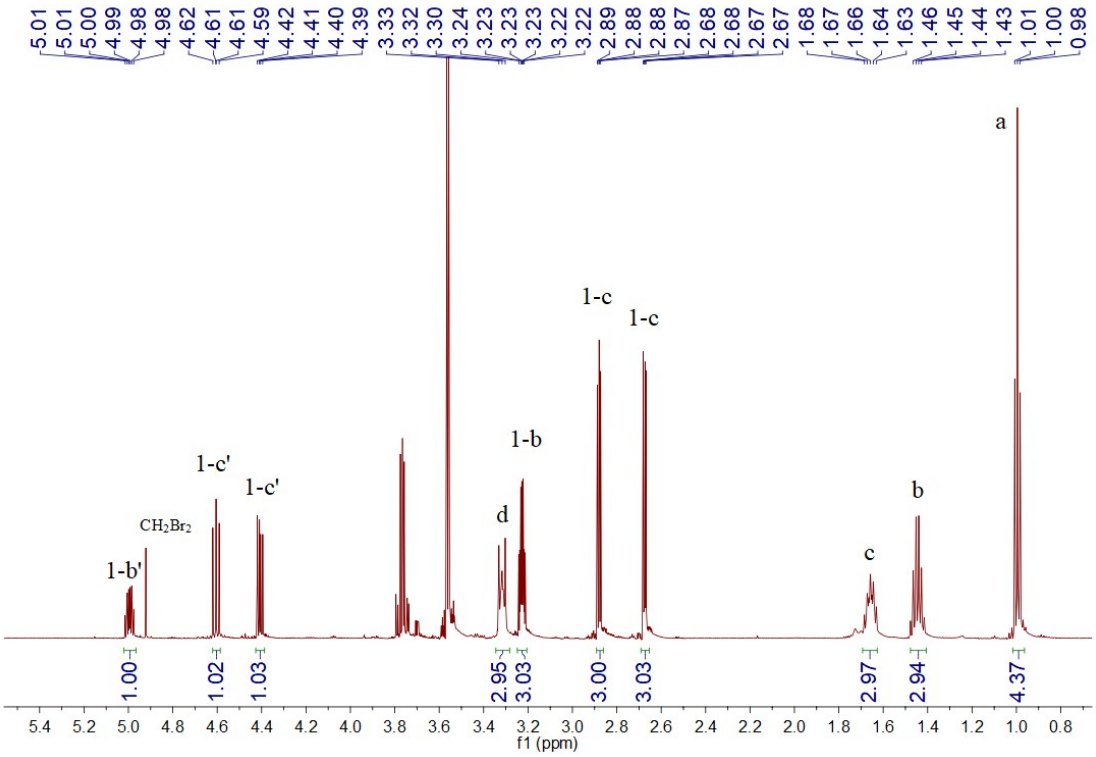

Figure S23. The first run of S-1-Cd-after spall as a catalyst in epichlorohydrin.

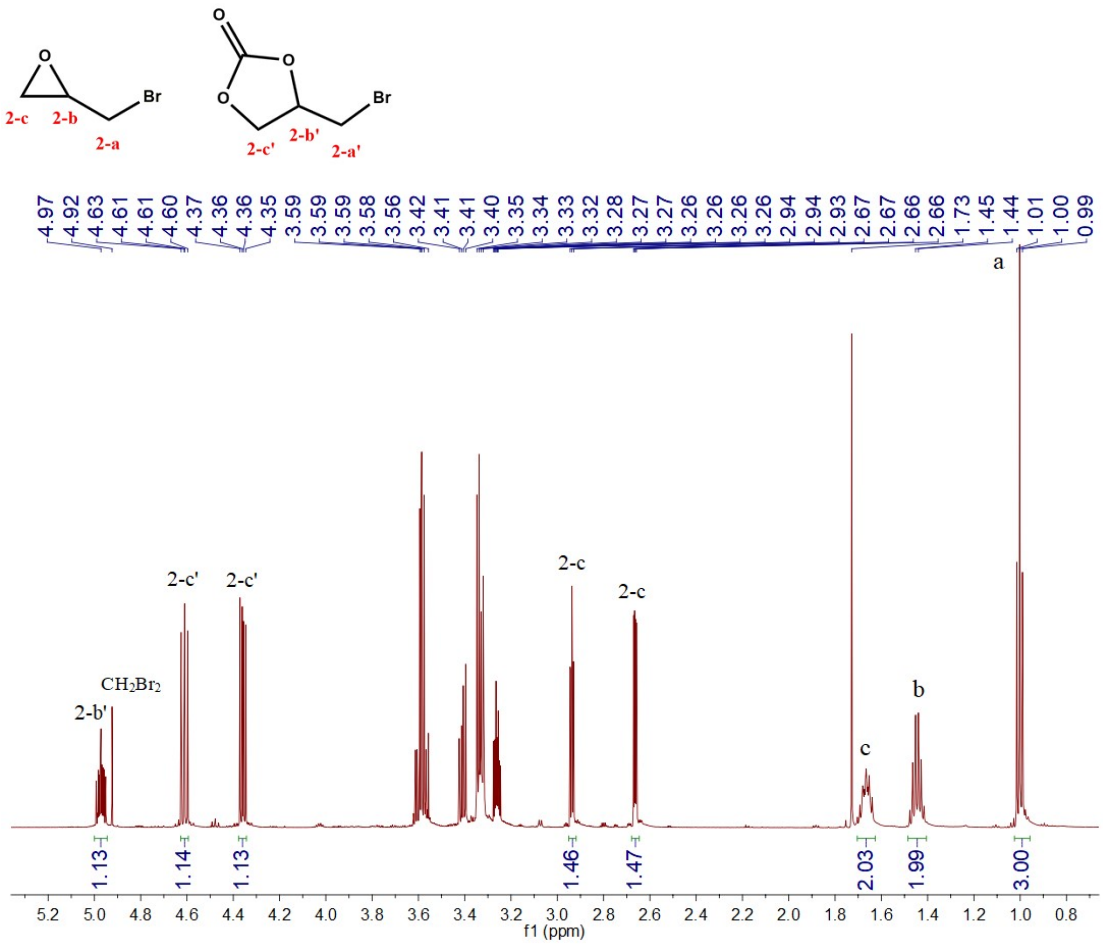

Figure S24. The first run of S-1-Zn-crystal as a catalyst in 1-Bromo-2,3-epoxypropane.

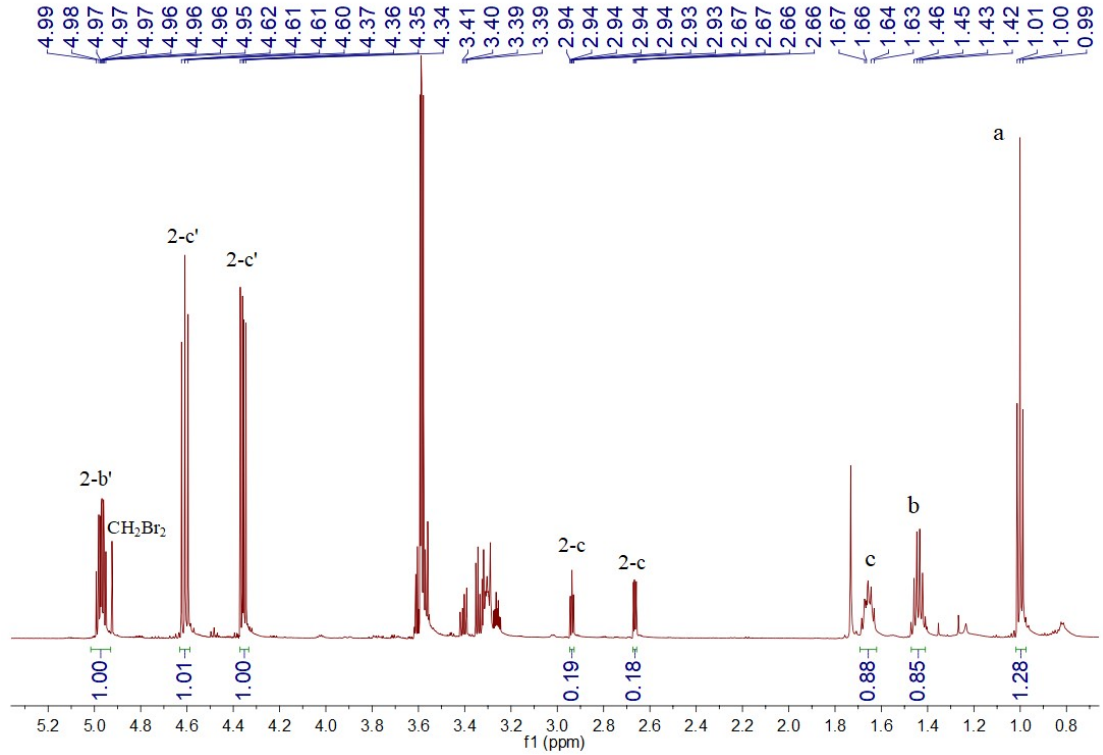

Figure S25. The first run of S-1-Zn-after spall as a catalyst in 1-Bromo-2,3-epoxypropane.

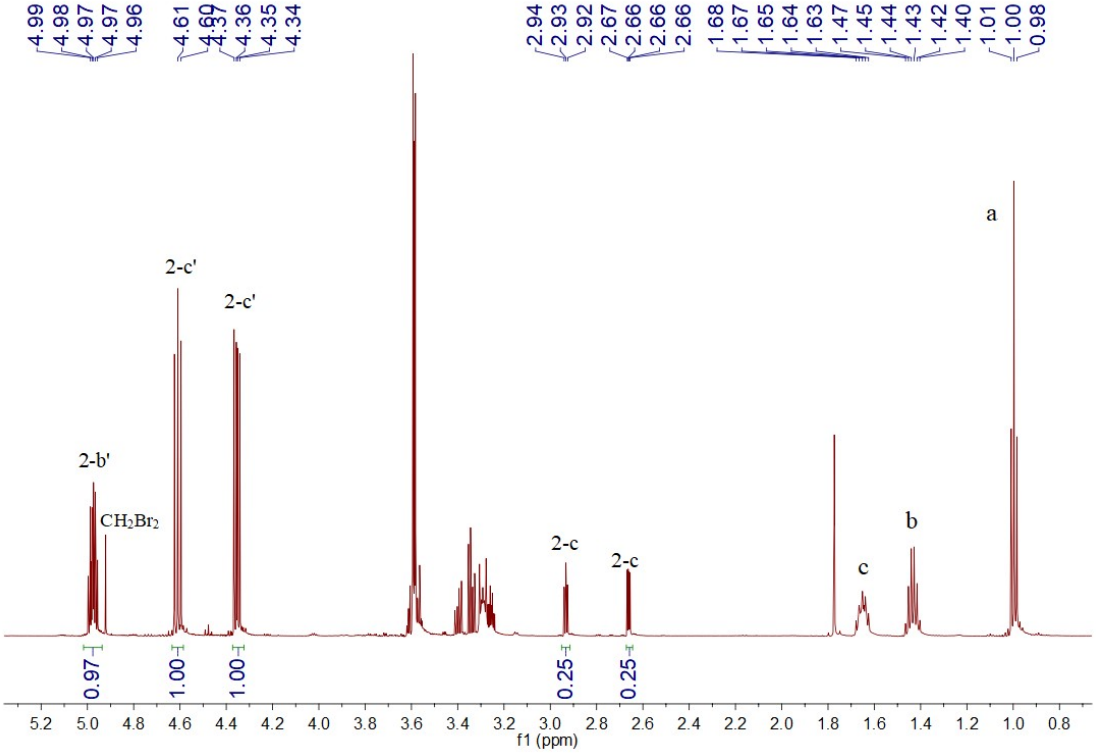

Figure S26. The second run of S-1-Zn-after spall as a catalyst in 1-Bromo-2,3-epoxypropane.

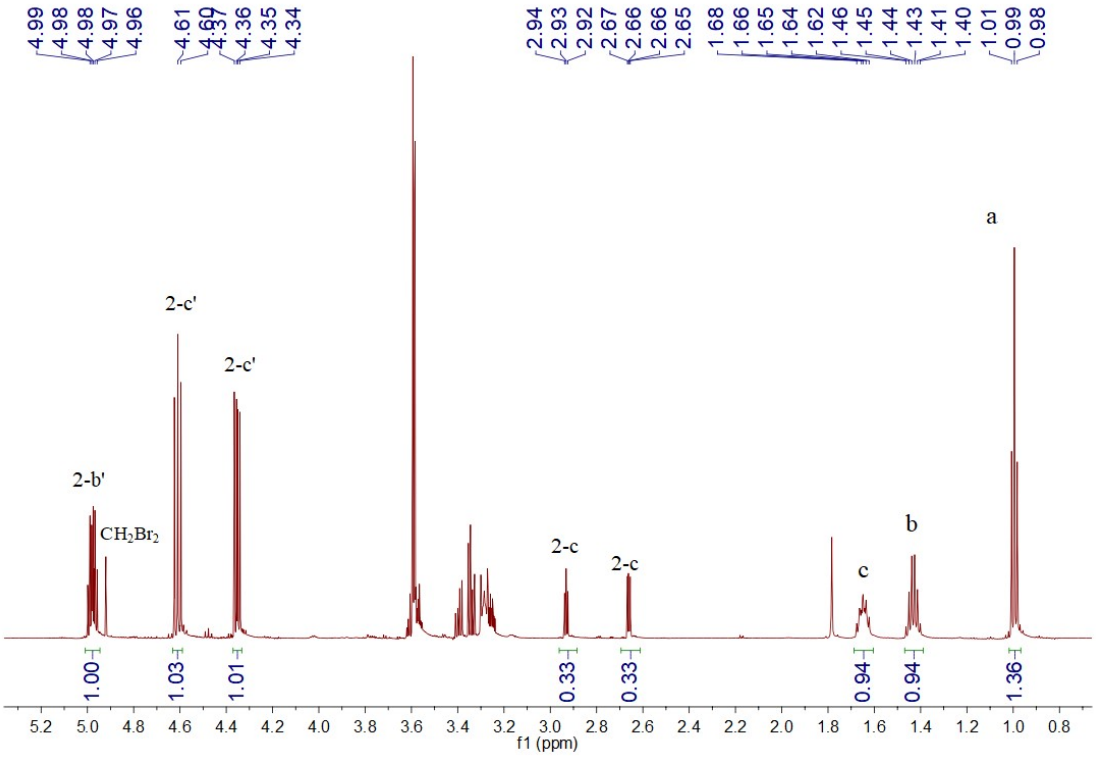

Figure S27. The third run of S-1-Zn-after spall as a catalyst in 1-Bromo-2,3-epoxypropane.

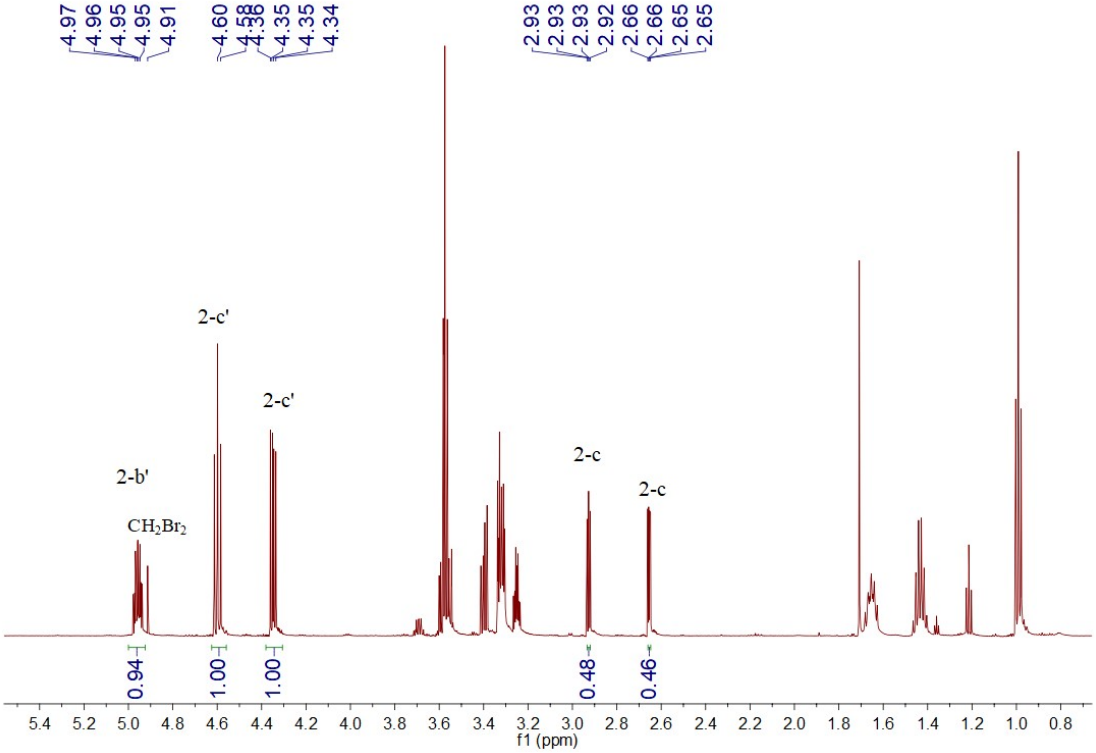

Figure S28. The fourth run of S-1-Zn-after spall as a catalyst in 1-Bromo-2,3-epoxypropane.

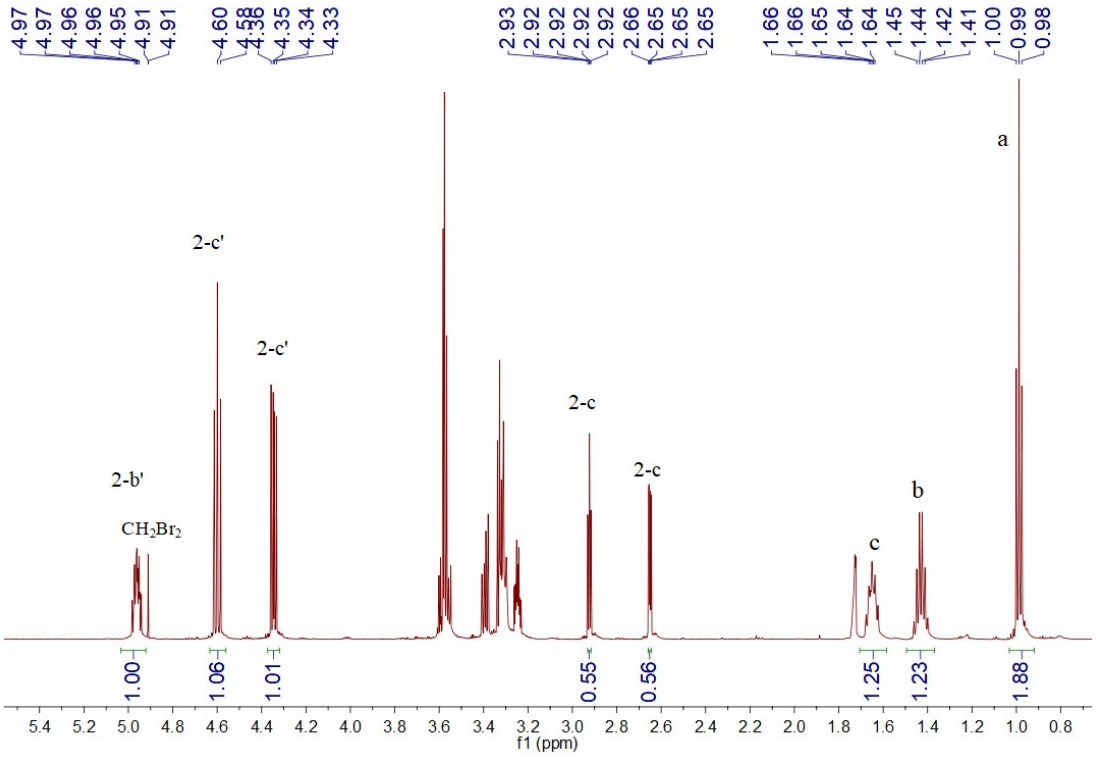

Figure S29. The fifth run of S-1-Zn-after spall as a catalyst in 1-Bromo-2,3-epoxypropane.

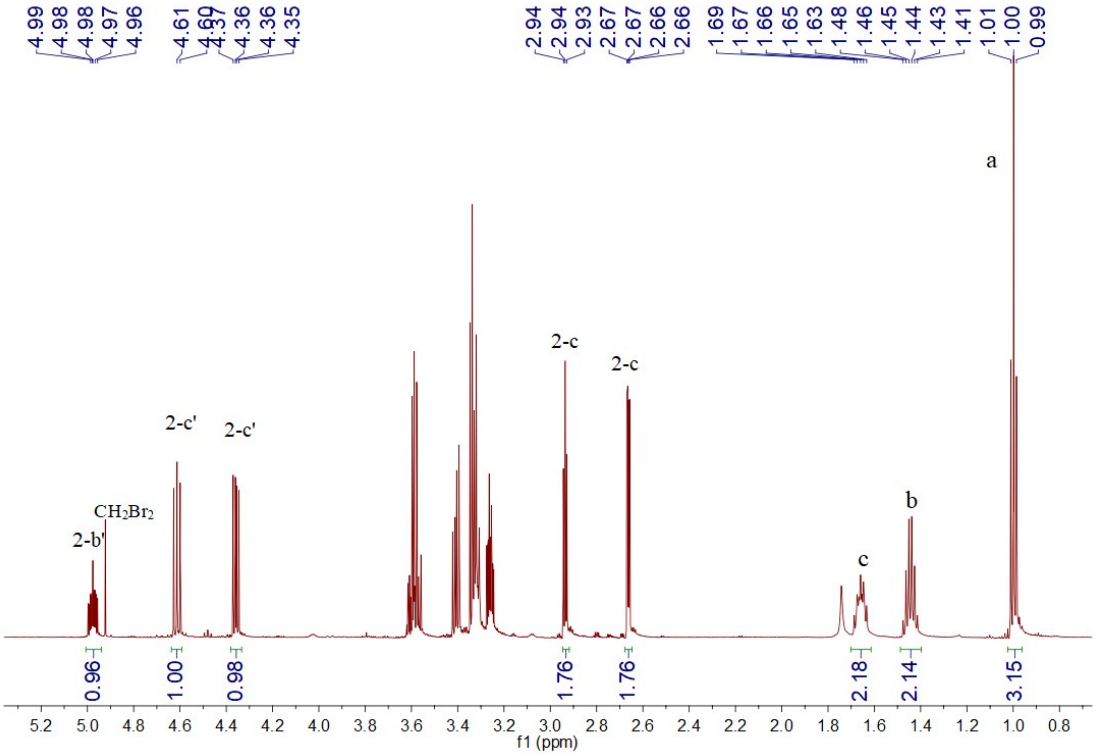

Figure S30. The first run of S-1-Cd-crystal as a catalyst in 1-Bromo-2,3-epoxypropane.

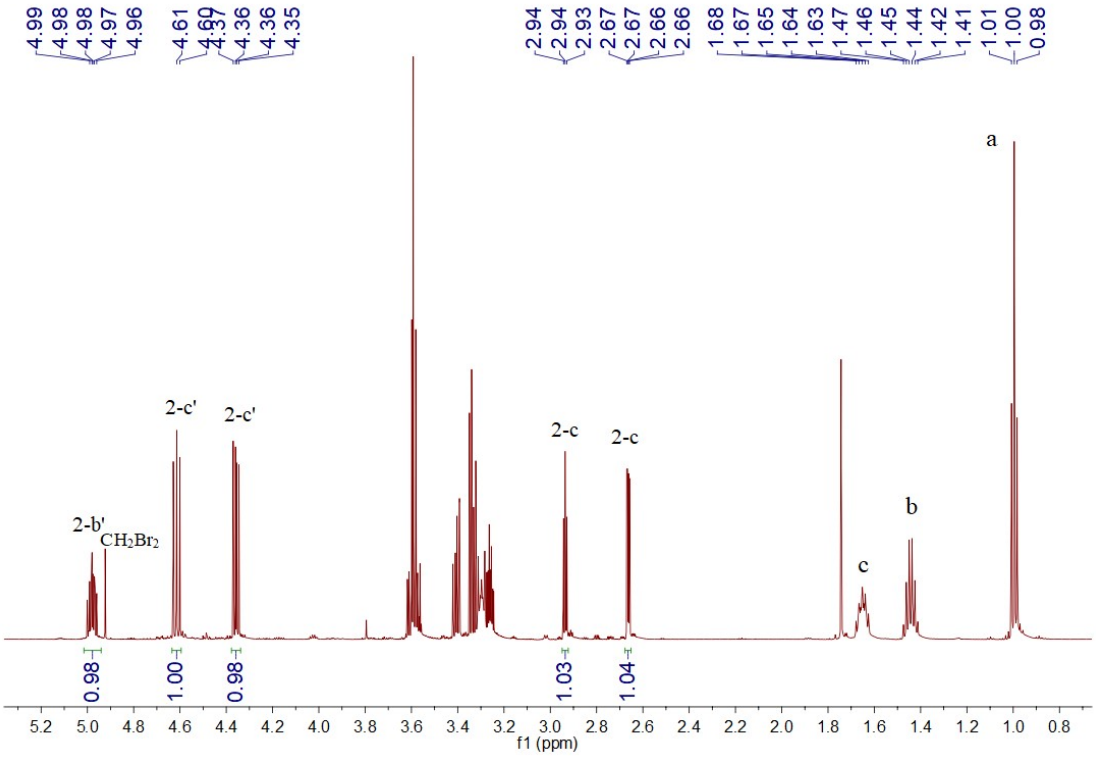

Figure S31. The first run of S-1-Cd-after spall as a catalyst in 1-Bromo-2,3-epoxypropane.

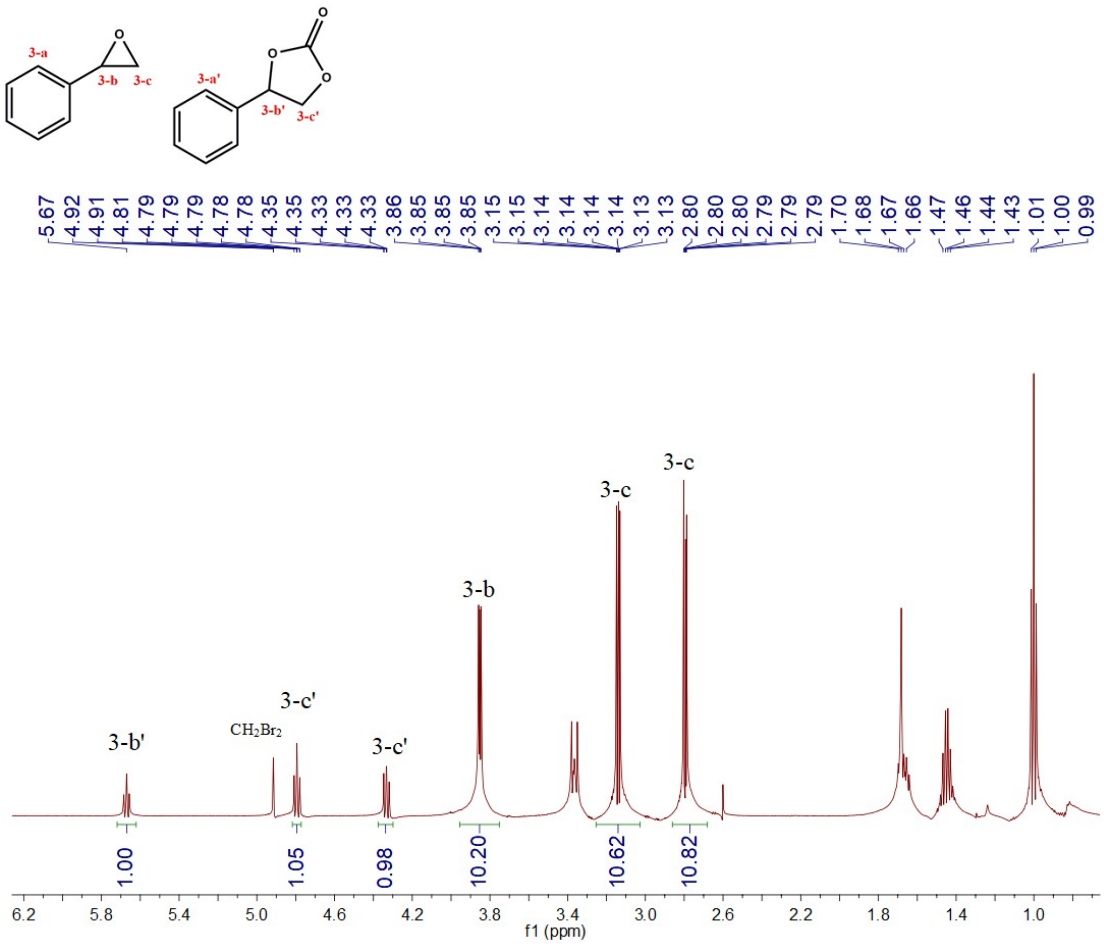

Figure S32. The first run of S-1-Zn-crystal as a catalyst in Styrene oxide.

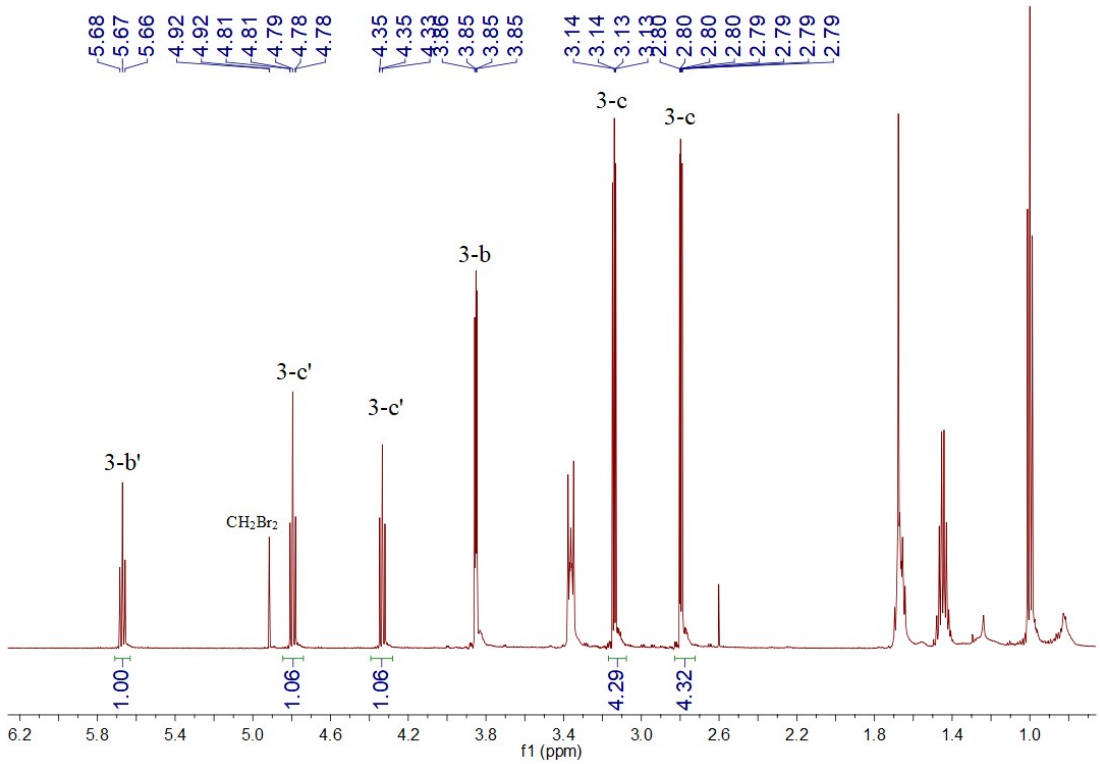

Figure S33. The first run of S-1-Zn-after spall as a catalyst in Styrene oxide.

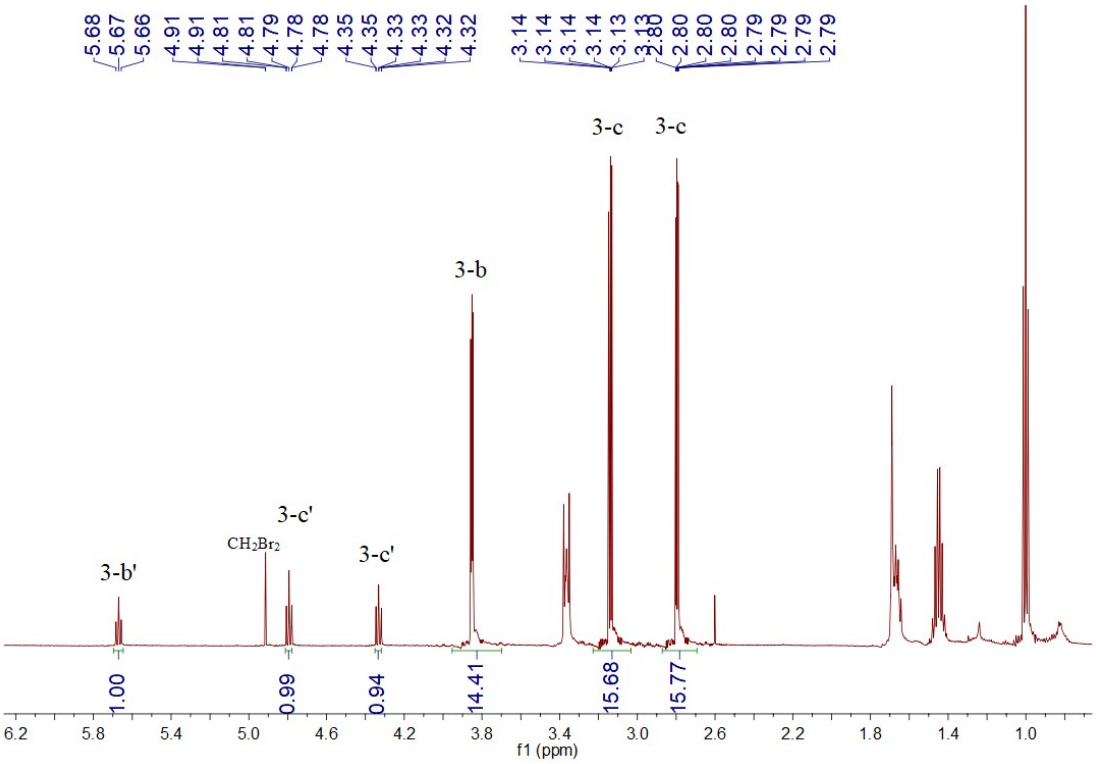

Figure S34. The first run of S-1-Cd-crystal as a catalyst in Styrene oxide.

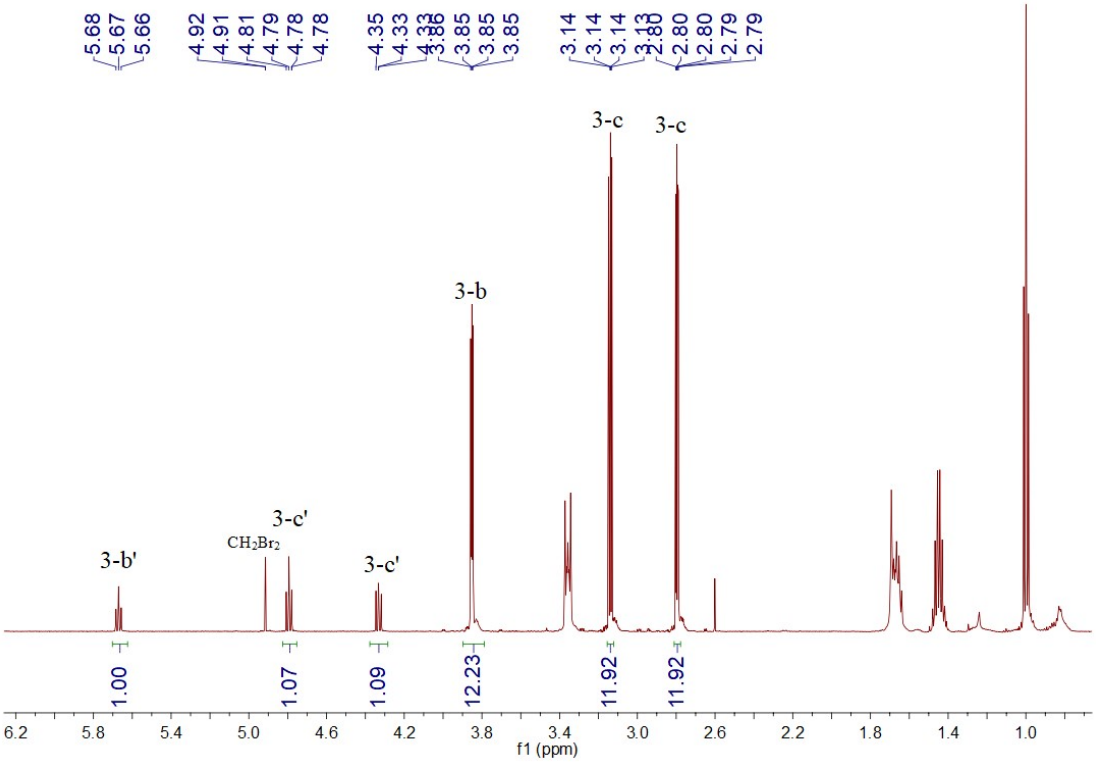

Figure S35. The first run of S-1-Cd-after spall as a catalyst in Styrene oxide.

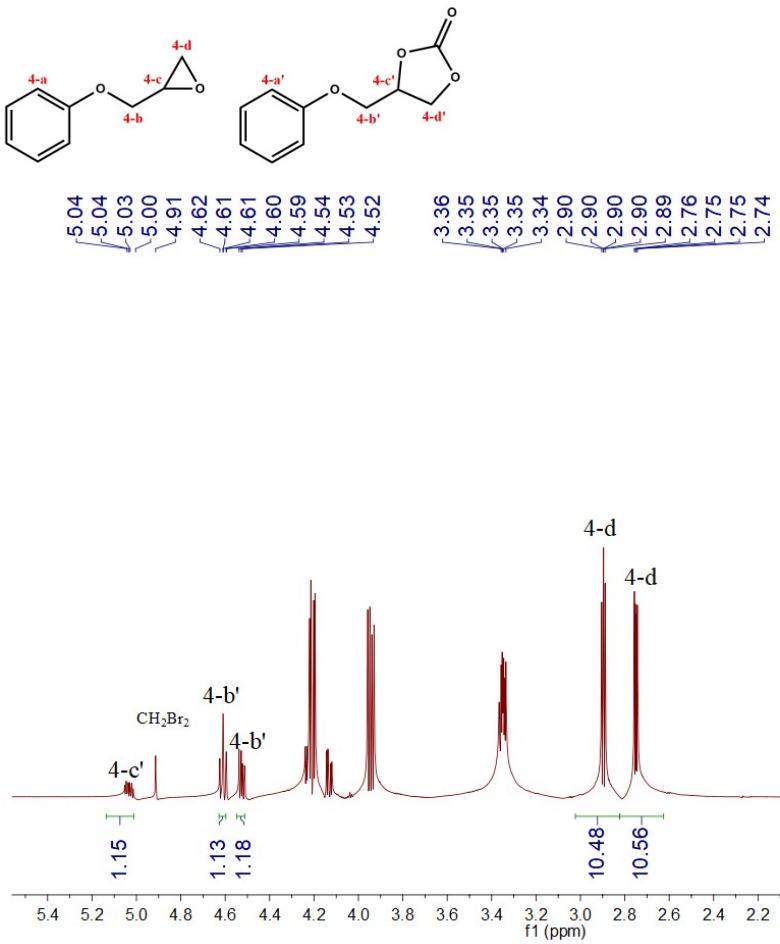

Figure S36 The first run of S-1-Zn-crystal as a catalyst in glycidyl phenyl ether.

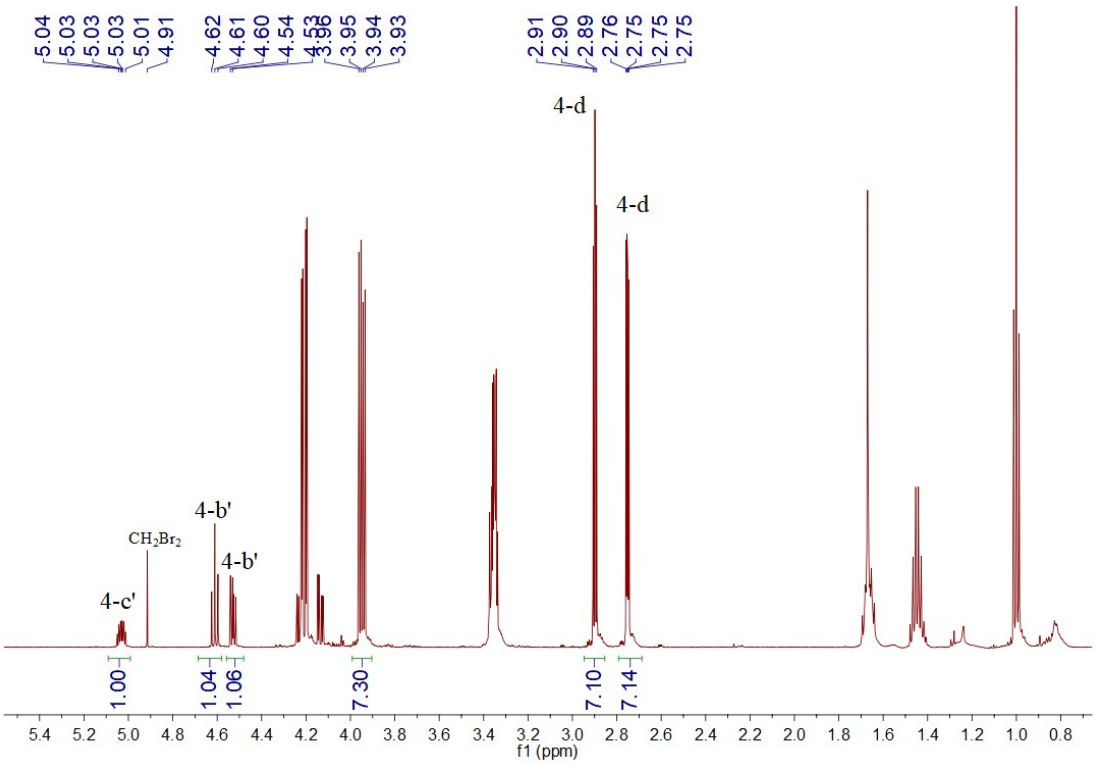

Figure S37. The first run of S-1-Zn-after spall as a catalyst in glycidyl phenyl ether.

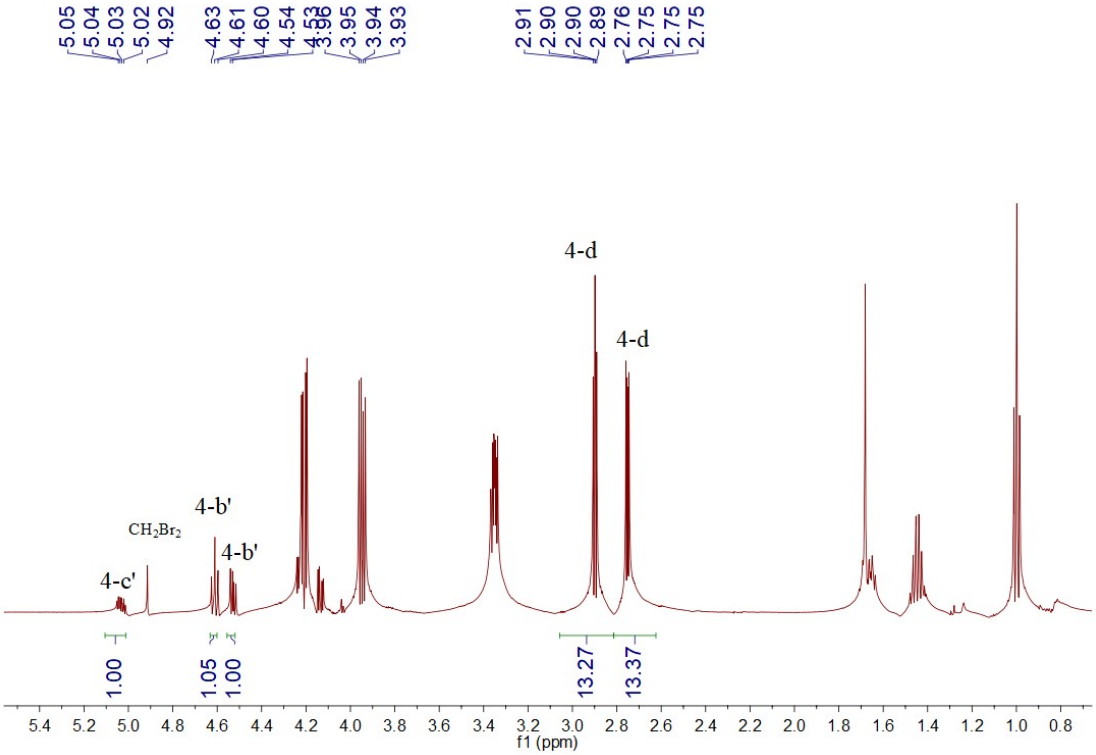

Figure S38. The first run of S-1-Cd-crystal as a catalyst in glycidyl phenyl ether.

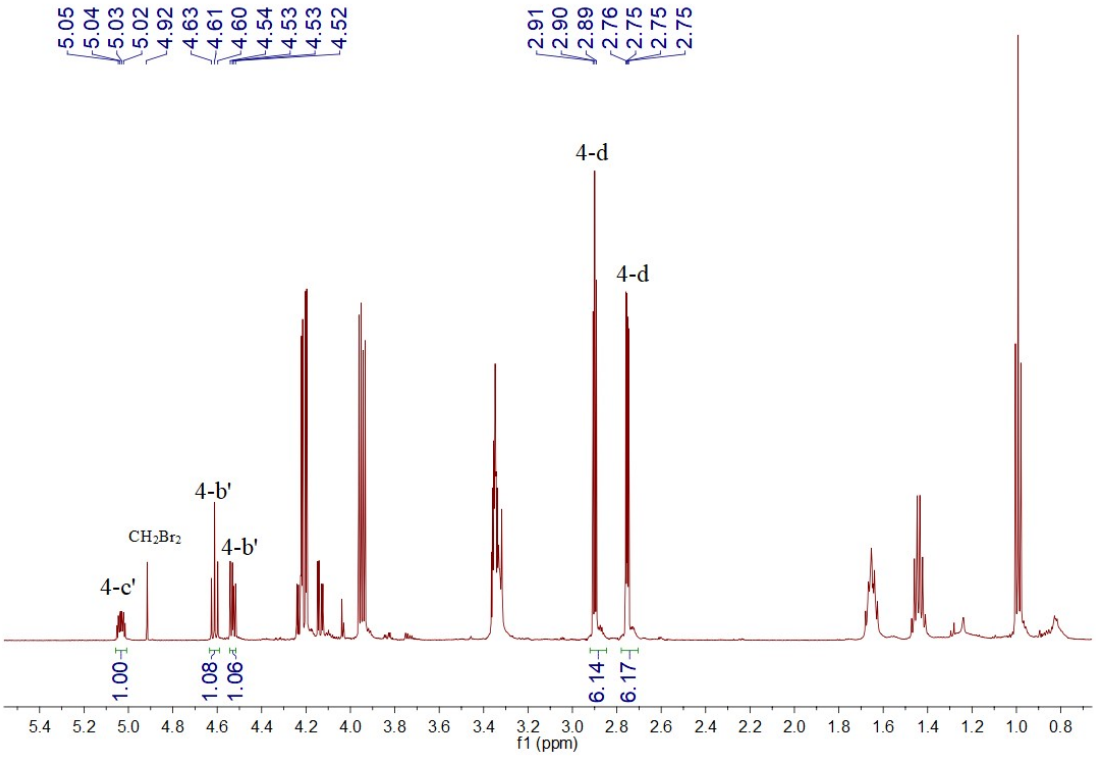

Figure S39. The first run of S-1-Cd-after spall as a catalyst in glycidyl phenyl ether.

Controlled experiment

Table S7. Only use TBAB as co-catalyst in the catalytic reaction of four substrates.

Substrate	Crystals	Co-catalyst	Yield (%)
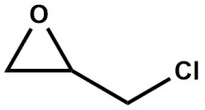	none	TBAB	**20.0**
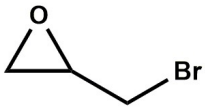	none	TBAB	**31.6**
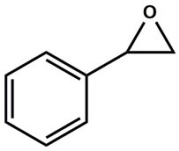	none	TBAB	**3.6**
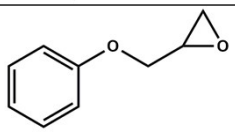	none	TBAB	**5.5**

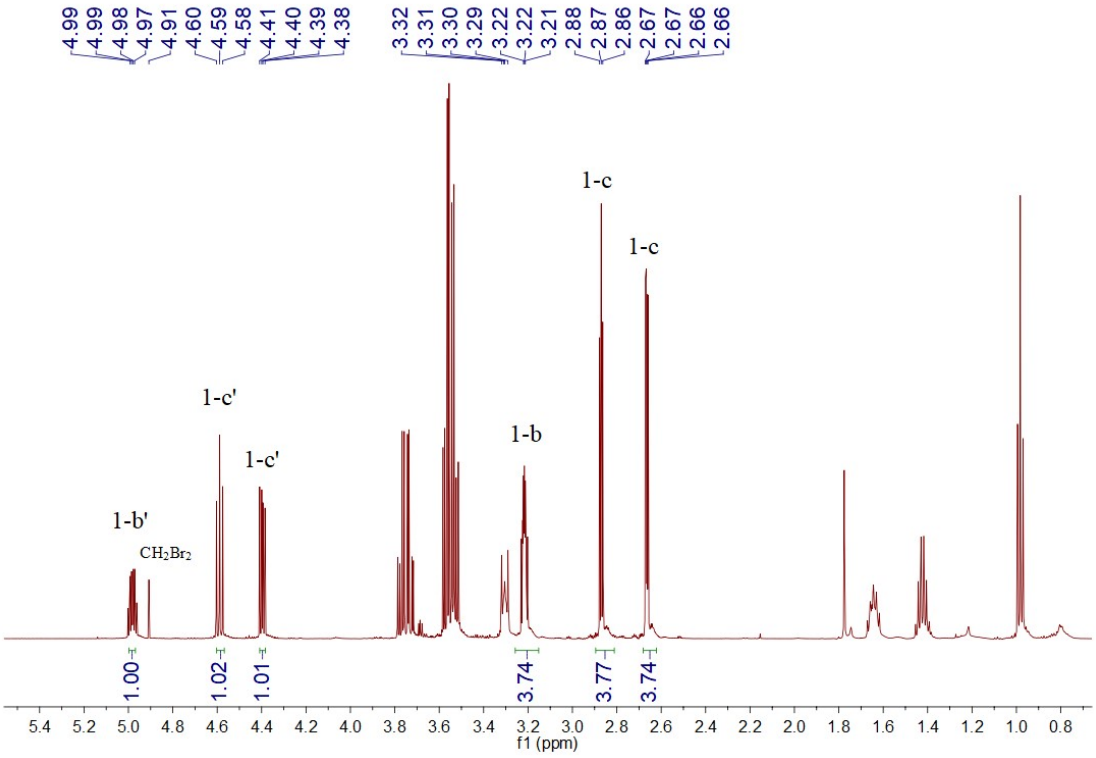

Figure S40. Only TBAB as co-catalyst in epichlorohydrin.

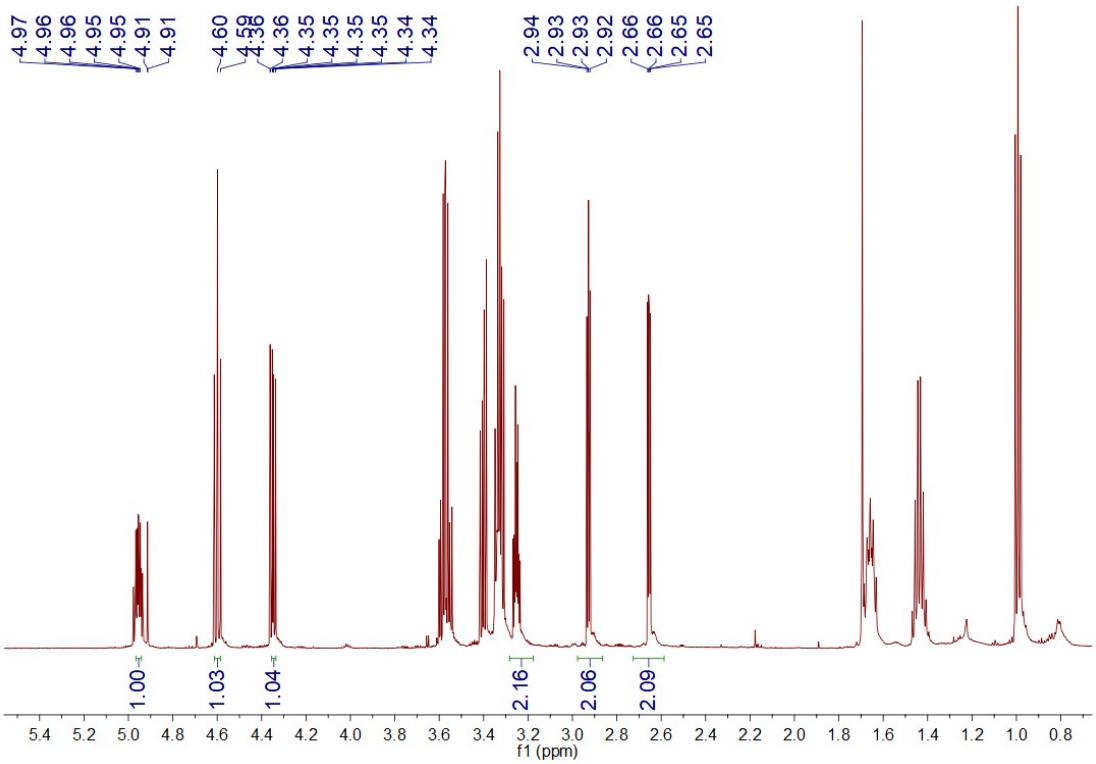

Figure S41. Only TBAB as co-catalyst in 1-Bromo-2,3-epoxypropane.

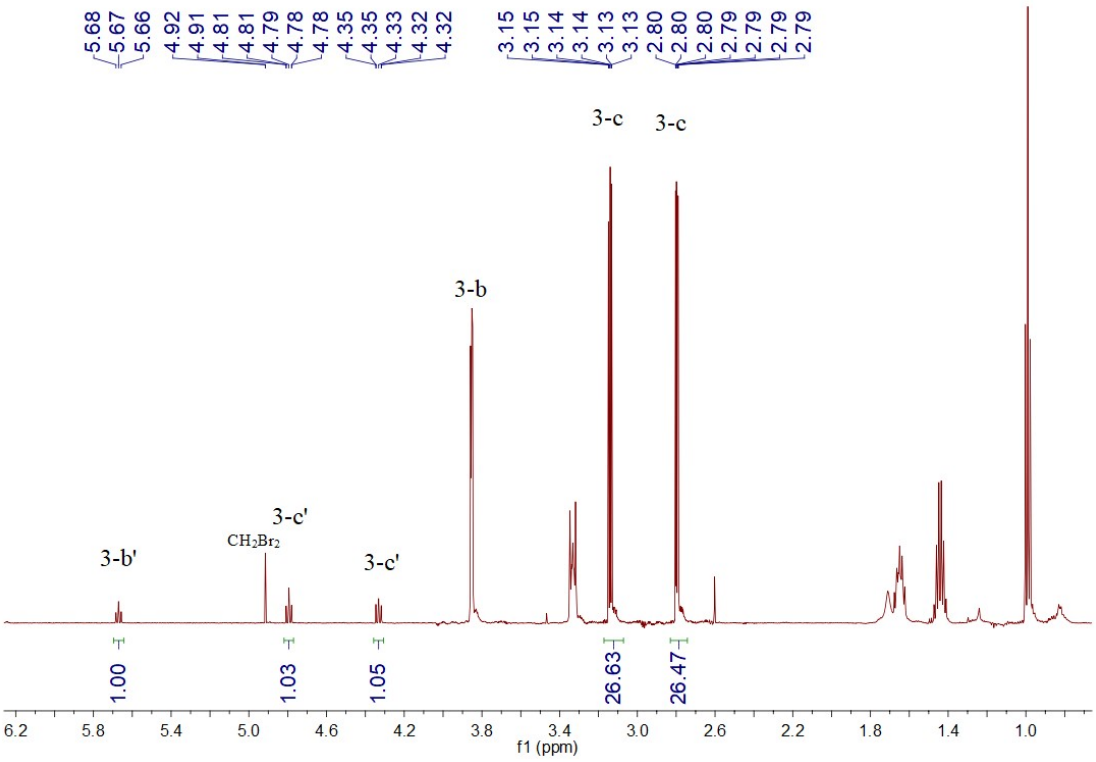

Figure S42. Only TBAB as co-catalyst in Styrene oxide.

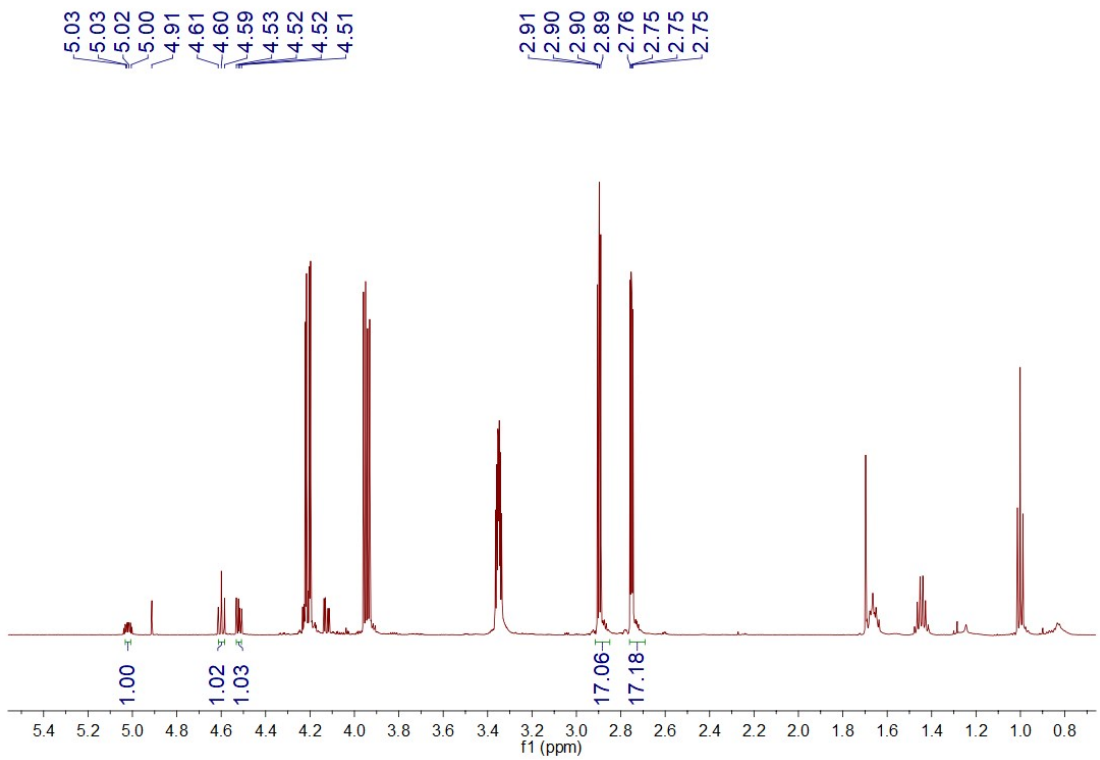

Figure S43. Only TBAB as co-catalyst in glycidyl phenyl ether.

Co-catalyst comparison

Table S8. Only use S-1-Zn-crystal as a catalyst in the catalytic reaction of four co-catalysts.

Substrate	TBAF	TBACl	TBAB	TBAI
	4.8	**35.1**	**30.1**	**31.0**
	39.8	**75.7**	**42.5**	**63.3**

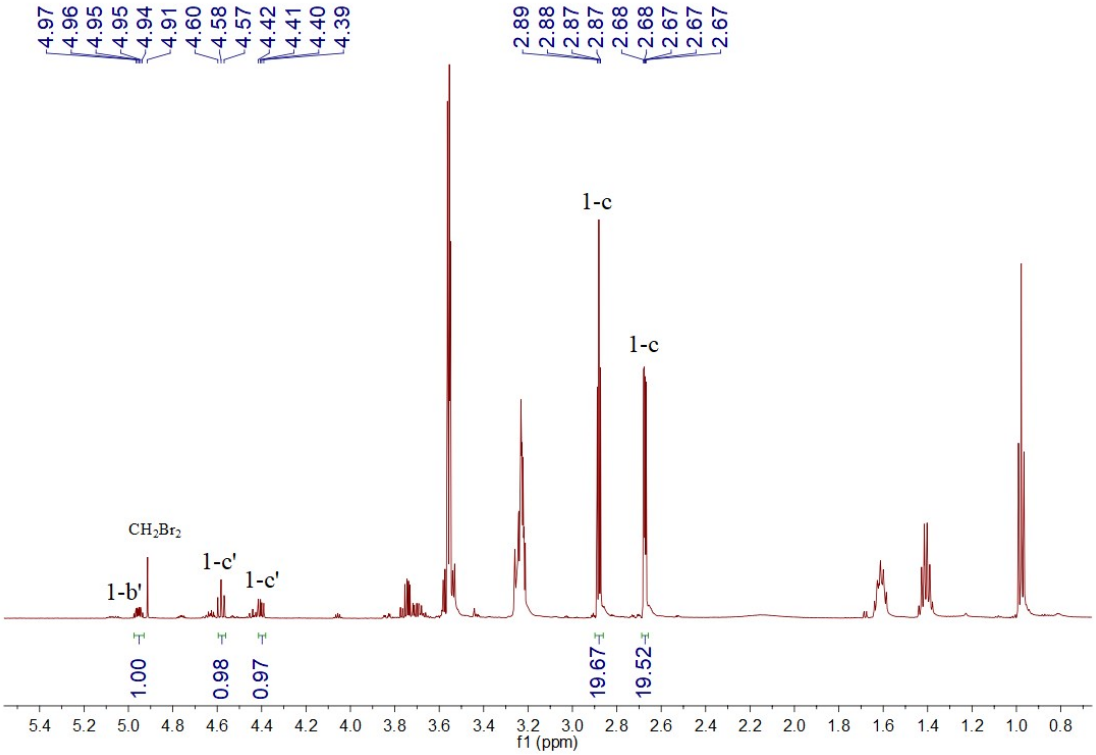

Figure S44. The TBAF as co-catalyst and S-1-Zn-crystal as a catalyst in epichlorohydrin.

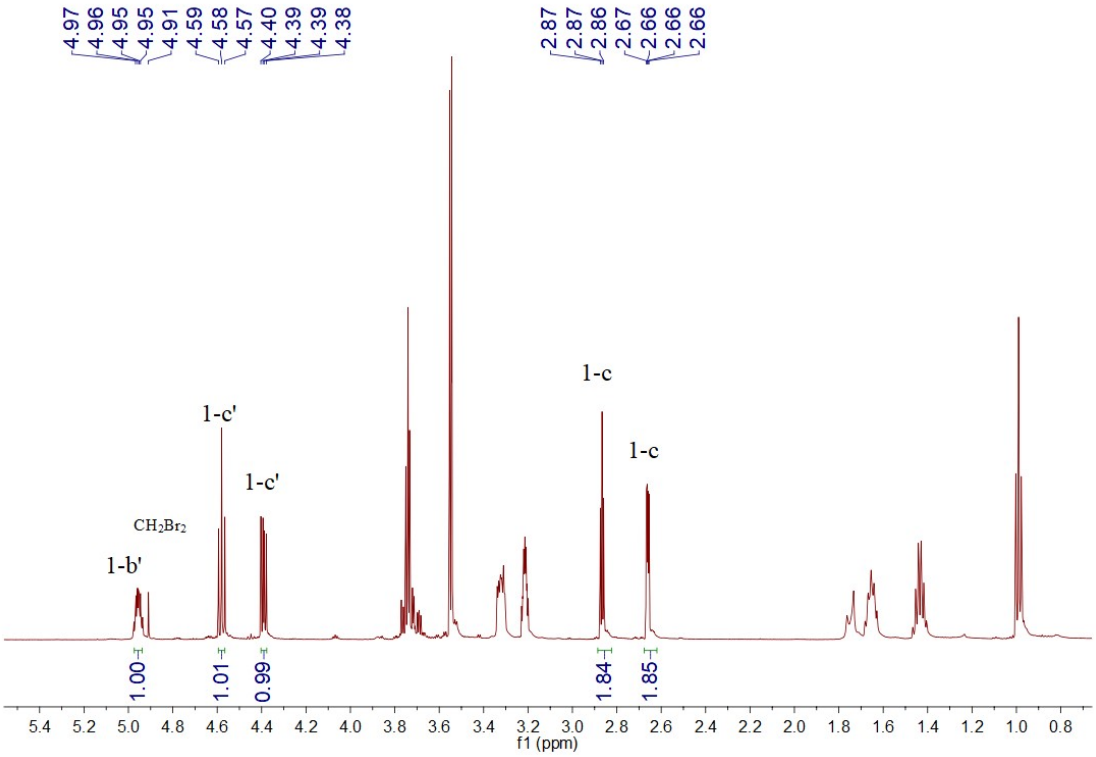

Figure S45. The TBACl as co-catalyst and S-1-Zn-crystal as a catalyst in epichlorohydrin.

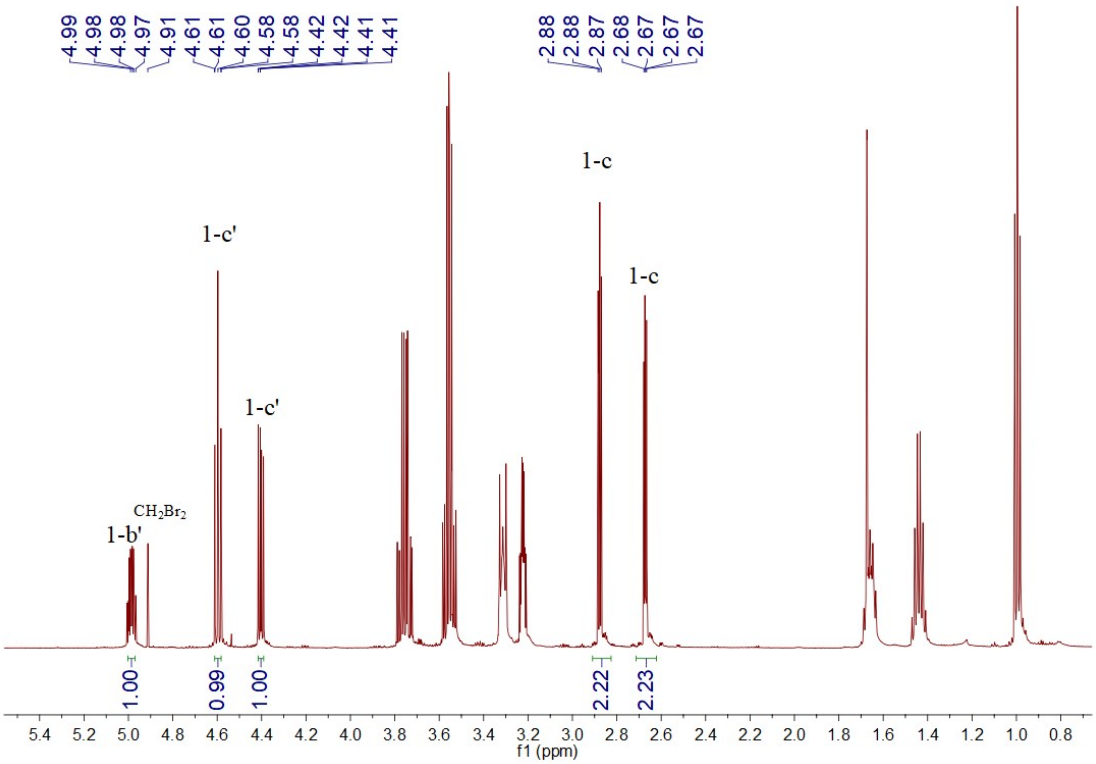

Figure S46. The TBAI as co-catalyst and S-1-Zn-crystal as a catalyst in epichlorohydrin.

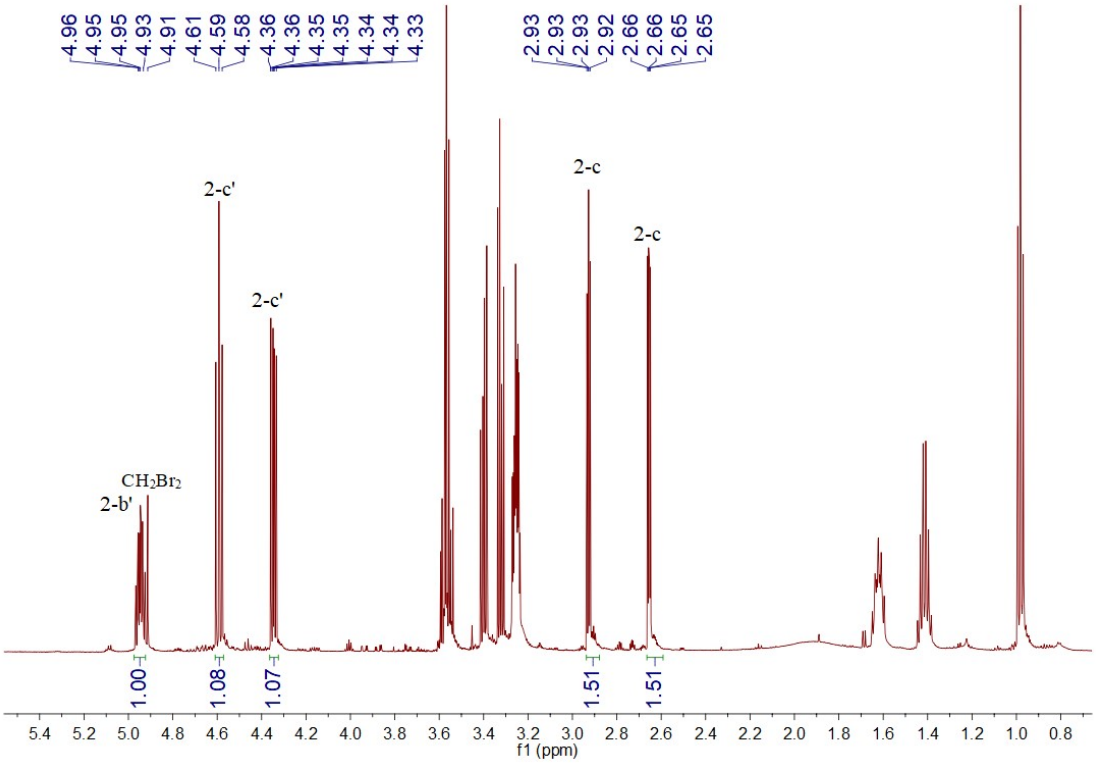

Figure S47. The TBAF as co-catalyst and S-1-Zn-crystal as a catalyst in 1-Bromo-2,3-epoxypropane.

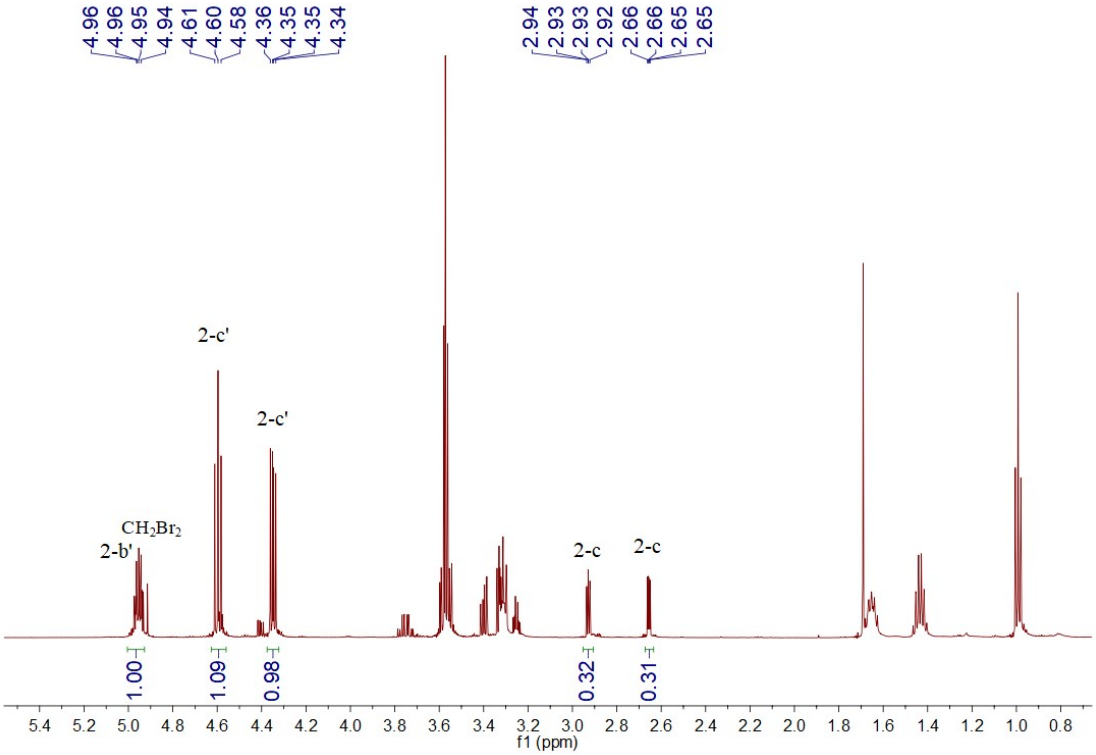

Figure S48. The TBACl as co-catalyst and S-1-Zn-crystal as a catalyst in 1-Bromo-2,3-epoxypropane.

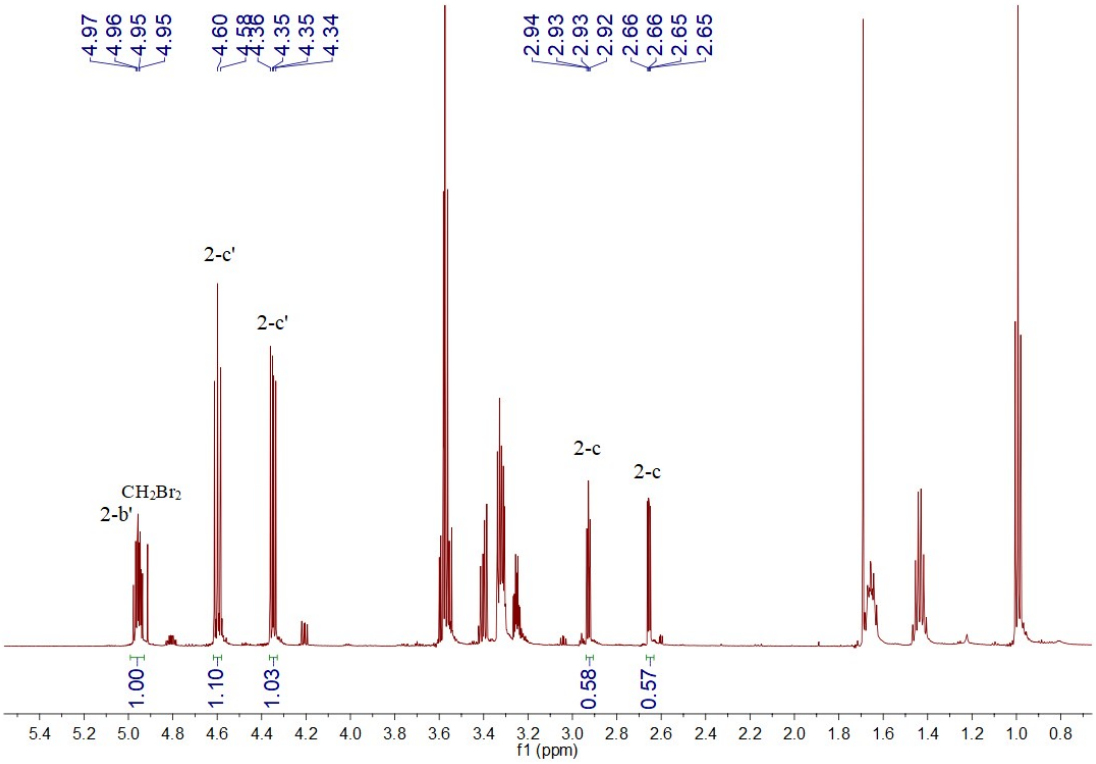

Figure S49. The TBAI as co-catalyst and S-1-Zn-crystal as a catalyst in 1-Bromo-2,3-epoxypropane.

Reference

[1] Li X Y, Ma L N, Liu Y, et al. Honeycomb metal–organic framework with lewis acidic and basic bifunctional sites: selective adsorption and CO2 catalytic fixation[J]. ACS applied materials & interfaces, 2018, 10(13): 10965-10973.

[2] Gong Y N, Liu J W, Mei J H, et al. Incorporation of Chromophores into Metal–Organic Frameworks for Boosting CO2 Conversion[J]. Inorganic Chemistry, 2021, 60(19): 14924-14931.

[3] Zhang S, Zhang H, Cao F, et al. Catalytic behavior of graphene oxides for converting CO2 into cyclic carbonates at one atmospheric pressure[J]. ACS Sustainable Chemistry & Engineering, 2018, 6(3): 4204-4211.

[4] Yao C, Zhou S, Kang X, et al. A cationic zinc–organic framework with Lewis acidic and basic bifunctional sites as an efficient solvent-free catalyst: CO2 fixation and Knoevenagel condensation reaction[J]. Inorganic Chemistry, 2018, 57(17): 11157-11164.

[5] Zhang B, Guo P Y, Ma L N, et al. Two Robust In (III)-Based Metal–Organic Frameworks with Higher Gas Separation, Efficient Carbon Dioxide Conversion, and Rapid Detection of Antibiotics[J]. Inorganic Chemistry, 2020, 59(7): 5231-5239.

[6] Wang W J, Liu J, Yan Y T, et al. Uncommon thioether-modified metal–organic frameworks with unique selective CO 2 sorption and efficient catalytic conversion[J]. CrystEngComm, 2021, 23(6): 1447-1454.

[7] Shao D, Shi J, Zhang J, et al. Solvent impedes CO2 cycloaddition on metal–organic frameworks[J]. Chemistry–An Asian Journal, 2018, 13(4): 386-389.

[8] Ng C K, Toh R W, Lin T T, et al. Metal–salen molecular cages as efficient and recyclable heterogeneous catalysts for cycloaddition of CO 2 with epoxides under ambient conditions[J]. Chemical science, 2019, 10(5): 1549-1554.

[9] Guo Z, Xu Y, Chao J, et al. Lithium organoaluminate complexes as catalysts for the conversion of CO2 into cyclic carbonates[J]. European Journal of Inorganic Chemistry, 2020, 2020(29): 2835-2841.

[10] Li P Z, Wang X J, Liu J, et al. A triazole-containing metal–organic framework as a highly effective and substrate size-dependent catalyst for CO2 conversion[J]. Journal of the American Chemical Society, 2016, 138(7): 2142-2145.

[11] Liang J, Huang Y B, Cao R. Metal–organic frameworks and porous organic polymers for sustainable fixation of carbon dioxide into cyclic carbonates[J]. Coordination Chemistry Reviews, 2019, 378: 32-65.

[12] Tombesi A, Pettinari C. Metal Organic Frameworks as Heterogeneous Catalysts in Olefin Epoxidation and Carbon Dioxide Cycloaddition[J]. Inorganics, 2021, 9(11): 81.